Research paper

6-Arylthio-3-hydroxypyrimidine-2,4-diones potently inhibited HIV reverse transcriptase-associated RNase H with antiviral activity

Lei Wang [a], Jing Tang [a], Andrew D. Huber [b], Mary C. Casey [c], Karen A. Kirby [c, d], Daniel J. Wilson [a], Jayakanth Kankanala [a], Jiashu Xie [a], Michael A. Parniak [e], Stefan G. Sarafianos [c, d, f], Zhengqiang Wang [a, *]

[a] Center for Drug Design, Academic Health Center, University of Minnesota, Minneapolis, MN, 55455, USA
[b] Department of Veterinary Pathobiology, College of Veterinary Medicine, University of Missouri, Christopher S. Bond Life Sciences Center, Columbia, MO, 65211, USA
[c] Department of Molecular Microbiology and Immunology, University of Missouri School of Medicine, Christopher S. Bond Life Sciences Center, Columbia, MO, 65211, USA
[d] Laboratory of Biochemical Pharmacology, Department of Pediatrics, Emory University School of Medicine, Atlanta, GA, 30322, USA
[e] Department of Microbiology & Molecular Genetics, University of Pittsburgh School of Medicine, Pittsburgh, PA, 15219, USA
[f] Department of Biochemistry, University of Missouri, Christopher S. Bond Life Sciences Center, Columbia, MO, 65211, USA

ARTICLE INFO

ABSTRACT

Human immunodeficiency virus (HIV) reverse transcriptase (RT) associated ribonuclease H (RNase H) remains the only virally encoded enzymatic function not targeted by current drugs. Although a few chemotypes have been reported to inhibit HIV RNase H in biochemical assays, their general lack of significant antiviral activity in cell culture necessitates continued efforts in identifying highly potent RNase H inhibitors to confer antiviral activity. We report herein the design, synthesis, biochemical and antiviral evaluations of a new 6-arylthio subtype of the 3-hydroxypyrimidine-2,4-dione (HPD) chemotype. In biochemical assays these new analogues inhibited RT RNase H in single-digit nanomolar range without inhibiting RT polymerase (pol) at concentrations up to $10\,\mu M$, amounting to exceptional biochemical inhibitory selectivity. Many analogues also inhibited integrase strand transfer (INST) activity in low to sub micromolar range. More importantly, most analogues inhibited HIV in low micromolar range without cytotoxicity. In the end, compound **13j** (RNase H $IC_{50} = 0.005\,\mu M$; RT pol $IC_{50} = 10\,\mu M$; INST $IC_{50} = 4.0\,\mu M$; antiviral $EC_{50} = 7.7\,\mu M$; $CC_{50} > 100\,\mu M$) represents the best analogues within this series. These results characterize the new 6-arylthio-HPD subtype as a promising scaffold for HIV RNase H inhibitor discovery.

1. Introduction

HIV antiviral therapy relies primarily on inhibitors of three virally encoded enzymes: RT, integrase (IN), and protease (PR) [1]. Combinations of these inhibitors form the highly active antiretroviral therapy (HAART), which renders HIV infection clinically manageable [2]. However, current drugs do not cure HIV and HAART can be plagued by the selection of resistant viral strains after long term use. Therefore, antivirals with a novel molecular target and a distinct antiviral mechanism of action are constantly needed to provide new options for HAART in combating drug-resistant viruses. HIV RT has two distinct domains [3]: a pol domain which carries out both RNA-dependent and DNA-dependent viral DNA polymerization and is targeted by all currently known nucleoside RT inhibitors (NRTIs) [4] and non-nucleoside RT inhibitors (NNRTIs) [5]; and an RNase H domain [3,6] which is required to degrade the RNA strand from the RNA/DNA reverse transcription intermediate, and process both the tRNA primer for minus strand DNA synthesis and the polypurine tract (PPT) primer for plus strand DNA synthesis. Significantly, active site mutations associated with attenuated RNase H biochemical activity *in vitro* conferred reduced HIV replication in cell culture [7], suggesting that RNase H functions are essential for HIV genome replication and that small molecules with potent and selective

RNase H inhibition should inhibit HIV replication. Unfortunately, despite decades of medicinal chemistry efforts, compounds conferring antiviral activity *via* targeting RNase H have yet to enter clinical development of any stage. As such, HIV RT-associated RNase H remains unvalidated as a drug target.

A few chemotypes (Fig. 1, A) have been reported to inhibit RNase H in biochemical assays [8], including 2-hydroxyisoquinolinedione (HID, **1**) [9], β-thujaplicinol (**2**) [10], dihydroxycoumarin (**3**) [11], diketoacid (DKA) **4** [12], pyrimidinol carboxylic acid **5** [13], hydroxynaphthyridine **6** [14] and pyridopyrimidone **7** (Fig. 1, A) [15]. These inhibitor types all feature a chelating triad (magenta) for binding two divalent metal ions. Structurally more elaborate chemotypes **4**–**7** also contain a hydrophobic aromatic moiety (cyan), which generally leads to more potent and selective RNase H inhibition in *in vitro* biochemical assays. HIV RNase H and IN share a similar active site fold as well as divalent metal dependence for catalytic activity [16]. Therefore, the chelating triad and the hydrophobic aromatic moiety embedded in inhibitor types **4**–**7** as well as typical INSTIs [17,18] may represent the minimal pharmacophore requirements for RNase H inhibitors. Unfortunately, the potent *in vitro* biochemical inhibition of RNase H observed with these inhibitor types typically does not confer significant antiviral activity in cell culture, possibly reflecting a steep biochemical barrier of small molecules competing against much larger RNA/DNA substrates [15]. Achieving RNase H inhibition in cell culture remains a challenge and likely requires tight RNase H binding and improved biochemical RNase H inhibition. We have long been interested in discovering antiviral compounds targeting HIV RNase H. Our efforts based on the aforementioned pharmacophore model have led to the discovery of four distinct chemotypes (**8**–**11**, Fig. 1, B), including the redesigned HID subtype **8** [19], the hydroxypyridonecarboxylic acid (HPCA) chemotype **9** [20], the redesigned HPD subtype **10** [21], and the *N*-hydroxy thienopyrimidine-2,4-dione chemotype **11** [22]. Among these inhibitor types HPD subtype **10** did not show appreciable HIV inhibition in cell culture despite potent and selective RNase H inhibition in *in vitro* biochemical assays [21]. Extended structure-activity relationship (SAR) analysis on **10** led to the design of subtypes **12** and **13** featuring a thio linkage at C-6 in lieu of the amino linkage (Fig. 1, C). Interestingly, **12** and **13** exhibited biochemical inhibitory profiles drastically different from that of **10**, as well as consistent antiviral activity in low micromolar range. We report herein the synthesis, biochemical and antiviral studies, and molecular modeling of **12** and **13**.
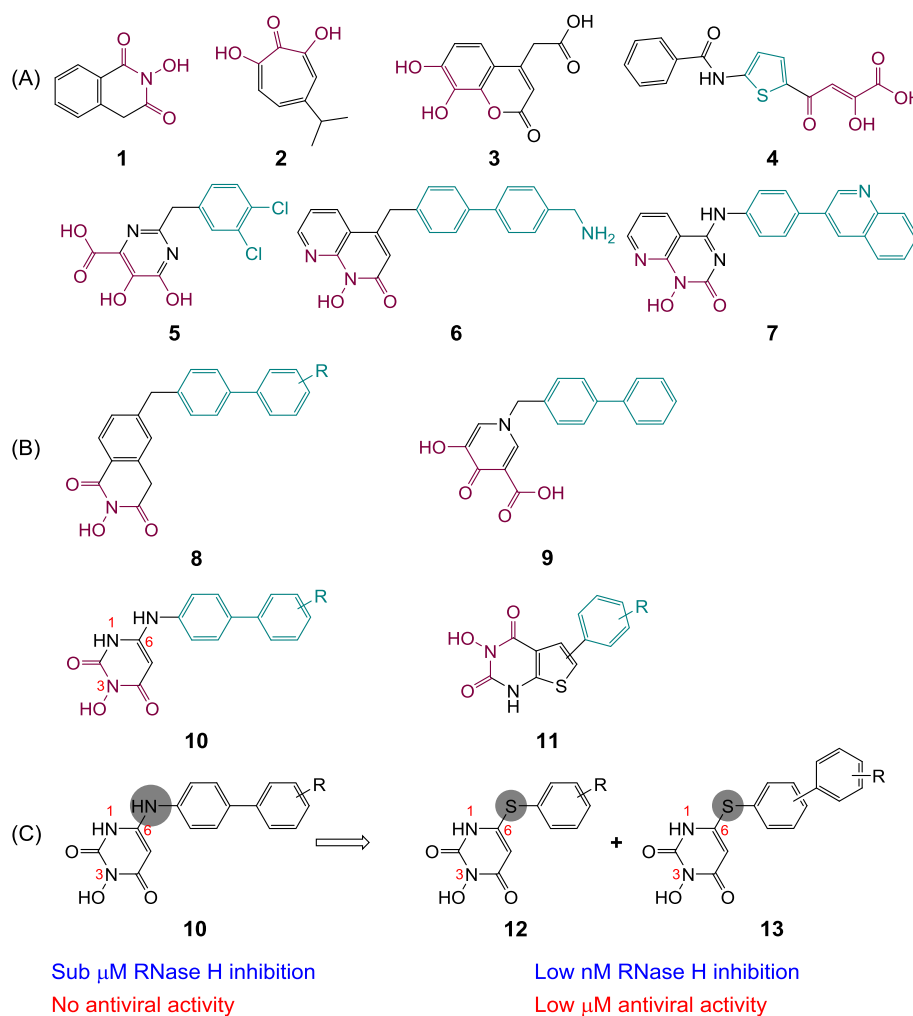

Fig. 1. Design of active site RNase H inhibitors. (A) Major chemotypes reported as HIV RNase H active site inhibitors. All chemotypes contain a chelating triad (magenta); scaffolds **4**–**7** also feature an aryl or biaryl moiety (cyan) connected through a methylene or amino linker; (B) our previously reported RNase H inhibitor chemotypes **8**–**11**; (C) the design of 6-phenylthio-HPD (**12**) and 6-biphenylthio-HPD (**13**) subtypes based on 6-biphenylamino-HPD (**10**). Subtypes **12** and **13** showed drastically improved biochemical potency *in vitro* and significant antiviral activity.

2. Results and discussion

2.1. Chemistry

Subtypes **12** and **20** were synthesized based on procedures adapted from the synthesis of **10** [21]. Commercially available hydroxyurea **14** was initially treated with BnBr in the presence of KOH, and the benzylated product **15** was subjected to cyclocondensation with diethyl malonate under microwave irradiation to afford six-membered heterocycle compound 3-(benzyloxy)-6-hydroxypyrimidine-2,4(1*H*, 3*H*)-dione **16** in good yield. Chlorination of **16** was carried out to give a key intermediate, 3-(benzyloxy)-6-chloropyrimidine-2,4(1*H*, 3*H*)-dione, **17** which was then treated with thiophenol in pyridine under microwave irradiation to produce 6-thio products **18** [23]. Finally, a TFA-mediated debenzylation allowed the synthesis of 21 analogues of subtype **12**. In the meantime, **18** can be brominated or iodinated to produce intermediates **19** which upon TFA-mediated debenzylation yielded two halogenated analogues **20** (Scheme 1).

The biphenylthio subtype **13** was synthesized *via* a reaction sequence described in Scheme 2. Bromo analogues of **18** were first subjected to a Suzuki coupling [24] with various phenylboronic acids to give intermediates **21** which were debenzylated under TFA to afford 27 analogues of subtype **13**.

2.2. Biology

All 45 final compounds of subtypes **12**, **20** and **13** were first evaluated in a biochemical assay measuring the catalytic activity of RT-associated RNase H. To gauge the biochemical inhibitory selectivity, they were also tested in two additional biochemical assays against RT pol and INST, respectively. In addition, analogues of subtypes **12** and **13** were also tested in a MAGI assay for antiviral activity against HIV-1 and cytotoxicity.

6-Arylthio HPD analogues inhibited the RNase H catalytic activity of RT in vitro with exceptional potency without inhibiting RT pol. In

biochemical assays separately measuring the RNase H and pol activities of full-length RT, analogues of 6-phenylthio HPD subtype **12** did not inhibit RT pol at concentrations up to 10 μM (Table 1), with the single exception of **12m** which inhibited RT pol with an IC_{50} of 7.0 μM. By contrast, all 21 analogues of **12** exhibited low nM inhibition against RT RNase H ($IC_{50} = 0.007-0.037$ μM). The high potency did not seem to be affected significantly by the mono substitution on the phenyl ring (**12a** *vs.* **12b-t**). Interestingly, when the substituent is Et (**12c-d**), Cl (**12k-l**), Br (**12m-o**), or OMe (**12r-t**), the site of substitution (ortho, meta or para) had virtually no impact on potency. However, when the substituent is a CF_3 (**12e-g**) or F (**12h-j**) group the para substitution conferred 2−3 fold of decrease in potency when compared to meta or ortho substitution. It should be noted that a naphthalene analogue showed single digit nM inhibition against RNase H (**12u**, $IC_{50} = 0.007$ μM). As for 6-biphenylthio HPD subtype **13**, most analogues inhibited RT RNase H with IC_{50} values in single digit nM range, reflecting an improvement in potency over subtype **12**. This is evident with direct comparison between analogues with the same substitution on the phenyl ring, such as **12b** ($IC_{50} = 0.033$ μM) vs **13b** ($IC_{50} = 0.006$ μM), **12h** ($IC_{50} = 0.037$ μM) vs **13e** ($IC_{50} = 0.006$ μM), and **12s** ($IC_{50} = 0.013$ μM) vs **13j** ($IC_{50} = 0.005$ μM). A notable exception is the analogue with a para-CF_3 substituent on the terminal phenyl ring (**13c**) which exhibited significantly less potency ($IC_{50} = 0.039$ μM) than the rest of series (**13b-n**). The reduced inhibition conferred by the para-CF_3 substituent is consistent with the SAR observed with subtype **12** (compound **12e**). Interestingly, disubstituted analogues (**13k-n**) did not exhibit improved potency over mono substituted ones, suggesting that the second substituent may not be necessary. In addition, no discernible difference was observed between para (**13a-n**) and meta (**13o-s**) biphenyls; however, ortho biphenyls (**13u-v**) conferred substantially reduced potency, presumably due to steric hindrance and reduced contact surface. Interestingly, inhibitory activity against RT pol was also observed with about half of the analogues of subtype **13** in single digit μM range ($IC_{50} = 3.2-10$ μM), indicating that the added phenyl
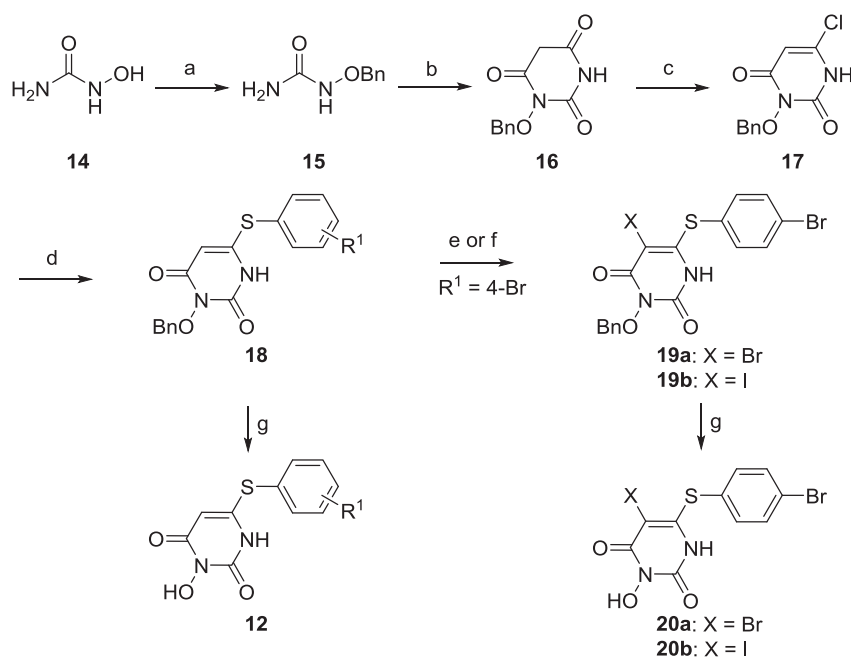
Scheme 1. ^a Synthesis of HPD subtypes **12** and **20**.

^a Reagents and conditions: (a) KOH, BnBr, MeOH, reflux, 6 h, 91%; (b) CH$_2$(COOEt)$_2$, NaOEt, microwave, 150 °C, 20 min, 58%; (c) POCl$_3$, BnEt$_3$NCl, 50 °C, 6 h, 78%; (d) thiophenol, pyridine, microwave, 140 °C, 40 min, 69−89%; (e) Br$_2$, MeOH, rt, 4 h (for **19a**); (f) Pb$_3$O$_4$, I$_2$, AcOH, 50 °C, overnight (for **19b**); (g) TFA, microwave, 120 °C, 40−50 min, 50−90%.
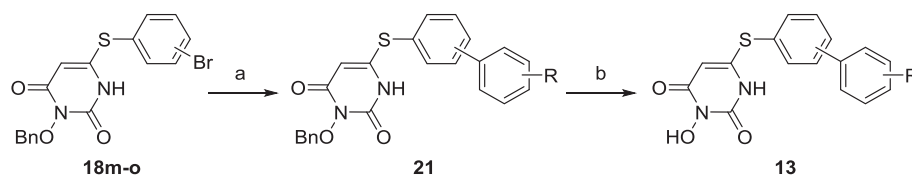
Scheme 2. [a] Synthesis of HPD subtype **13**.
[a] Reagents and conditions: (a) arylboronic acid, Pd(PPh$_3$)$_4$, K$_2$CO$_3$, MeOH/H$_2$O, microwave, 120 °C, 30–50 min, 40–79%; (b) TFA, microwave, 120 °C, 40–50 min, 39–90%.

ring also benefits binding to the RT pol domain, though pol inhibition is around three orders of magnitude lower than RNase H inhibition. Another important SAR observation was that halogenating the C-5 site drastically altered the RT inhibitory profile of subtype **12** as resulting analogues (**20a-b**) demonstrated substantially lower potency against RNase H and higher potency against pol than **12m**. This observation, along with reported pharmacophore model on HEPT type of NNRTIs [25], strongly suggests that C-5 modification should be avoided in order to achieve selective RNase H inhibition. Finally, the ultra potent RNase H inhibition and the exceptional selectivity over pol inhibition with the current 6-arylthio HPD subtypes **12** and **13** were unmatched by previously reported **7** or **10** (**13j** vs **10j**). Particularly, the consistent single digit nM RNase H inhibition in vitro by the biphenylthio HPD subtype **13** far exceeded the level of potency observed with reported chemotypes.

6-Arylthio HPD analogues inhibited HIV INST. In the biochemical assay measuring INST activity, most analogues of subtype **12** demonstrated INST inhibition in sub to low μM range (IC$_{50}$ = 0.49–8.4 μM). The SAR for INST inhibition was similar to RNase H inhibition in that para substitution by CF$_3$ (**12e** vs **12f-g**) or F (**12h** vs **12i-j**) conferred less inhibition than meta or ortho substitution. However, for subtype **13** most analogues either did not inhibit INST at concentrations up to 100 μM (**13d**, **13i**, **13u-v**), or did not behave well enough under the assay condition to allow accurate IC$_{50}$ measurement (**13b-c**, **13e-g**, **13j**, **13n-q**, **13s-t**). In the latter case, an estimation was provided to convey the general level of inhibition which is markedly lower than that of RNase H inhibition. The lack of INST inhibition by analogues with an ortho biphenyl (**13u-v**) was consistent with the observation from the RNase H assay, further implying that the orthobiphenyl moiety severely hampers target inhibition. Nevertheless, three analogues (**13h**, **13k** and **13r**) of subtype **13** did inhibit INST in submicromolar range (IC$_{50}$ = 0.17–0.33 μM), albeit with much lower potency than their single digit nM RNase H inhibition.

Importantly, our biochemical inhibitory profiling used two FDA-approved INST inhibitors raltegravir (RAL) and dolutegravir (DTG) as negative controls for the RNase H assay and positive controls for the INST assay. The observation that they both potently inhibited INST without inhibiting RNase H provides a strong validation to our biochemical assays. Altogether, these biochemical assays characterize our new 6-arylthio HPD subtypes **12** and **13** as ultra potent and largely selective inhibitors of RT RNase H in vitro.

6-Arylthio HPD analogues of subtypes **12** *and* **13** *consistently inhibited HIV-1.* To evaluate the antiviral potential of these compounds, the vast majority of analogues of subtypes **12** and **13** were tested in a MAGI antiviral assay. The results are listed in Table 2. To help understand the potential antiviral mechanism of action, the biochemical inhibitory profile, including potencies against both the RNase H and INST and a selectivity index (INST IC$_{50}$/RNase H IC$_{50}$), is also included in Table 2. From the MAGI assay, the most important observation was that 13 out of 21 analogues of subtype **12** and 18 out of 21 tested analogues of subtype **13** inhibited HIV-1 in low μM range (EC$_{50}$ = 4.7–18 μM) without cytotoxicity (CC$_{50}$ > 100 μM).

This is significant as reported RT RNase H inhibitors typically did not exhibit consistent antiviral activity. One could argue that the level of antiviral activity may merely reflect the secondary inhibitory activity against INST. However, analogues **13i** (EC$_{50}$ = 10 μM) and **13l** (EC$_{50}$ = 17 μM) inhibited HIV-1 without inhibiting INST at all (IC$_{50}$ > 100 μM). On the other hand, a few analogues with strong INST inhibition, such as **12b** (IC$_{50}$ = 2.8 μM), **12k** (IC$_{50}$ = 0.64 μM), **12p** (IC$_{50}$ = 3.4 μM), **13h** (IC$_{50}$ = 0.17 μM) and **13k** (IC$_{50}$ = 0.33 μM), did not inhibit HIV-1 (EC$_{50}$ > 20 μM). To determine if permeability is the deciding factor in their lack of antiviral activity, the above-mentioned analogues were subjected to a parallel artificial membrane permeability assay (PAMPA). Interestingly, **12p** and **13h** exhibited extremely poor permeability (Table 3), presumably due to the highly polar −NO$_2$ or −OH group, respectively. While the poor permeability is consistent with the lack of anti-HIV activity for **12p** and **13h**, the good permeability observed with another two analogues, **12b** and **13k**, indicates that permeability may not be the limiting factor and that the correlation between INST inhibition and antiviral activity may not be strong. This, along with the excellent overall selectivity in RNase H inhibition over INST inhibition in vitro (SI, Table 2), suggests that the observed antiviral activity may be due to the potent inhibition of RNase H. The discrepancy between the antiviral EC$_{50}$ and the RNase H inhibitory IC$_{50}$ may reflect the inherent biochemical barrier of small molecules competing against the tight binding nucleic acid substrates. Nevertheless, when compared to known RT RNase H inhibitor types such as **7** and **10**, the consistent antiviral activity and the exceptional biochemical inhibitory profile should render the current 6-arylthio HPD subtypes **12** and **13** vastly improved scaffolds for RT RNase H inhibitor discovery.

2.3. Molecular modeling

To illustrate the binding mode of our new chemotype, docking analysis was performed for both the HIV RNase H and PFV IN with Glide XP (version 6.4) [26,27] using two metal sites as a constraint. The predicted binding mode of compound **13q** within the active site of RNase H (PDB code: 5J1E [20,28]) suggests a potential interaction between the HPD core (the 2-C=O-3-OH-4-C=O chelating triad) and the two metal cofactors (Mg^{2+}) which are co-ordinated to the active site acidic residues D443, E478, D498 and D549. The molecular model also suggests a potential interaction between the keto group at the 2-position (2-C=O) of **13q** and the imidazole of the highly conserved H539, which could stabilize inhibitor positioning near the active site metal-chelating residues D443, E478, D498, and D549, all of which are crucial for RT RNase H activity. In addition, the biaryl moiety is positioned to possibly interact with K540 through π-alkyl interaction as well as other protein residues or nucleic acid substrate near the small hydrophobic region of the RNase H. This predicted binding mode conforms to the general pharmacophore of active site RNase H inhibitors, hence corroborating the active site inhibition mechanism (Fig. 2A).
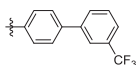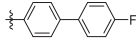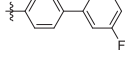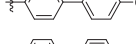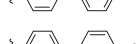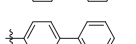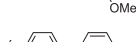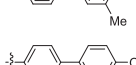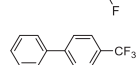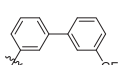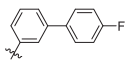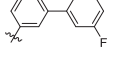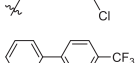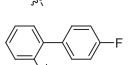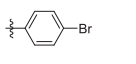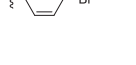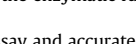
Molecular docking at the retroviral PFV IN active site was

Table 1
Biochemical inhibitory profile of subtypes **12**, **13** and **20** against HIV RNase H and pol activities of RT, and INST.

Compd	R^1	R^2	RT RNase H IC_{50}[a] (μM)	RT pol IC_{50}[a] (μM)	INST IC_{50}[a] (μM)
12a	H	phenyl	0.016 ± 0.002	>10	1.1 ± 0.3
12b	H	4-Me-phenyl	0.033 ± 0.003	>10	2.8 ± 0.6
12c	H	4-Et-phenyl	0.010 ± 0.0003	>10	1.3 ± 0.2
12d	H	2-Et-phenyl	0.010 ± 0.002	>10	0.75 ± 0.09
12e	H	4-CF_3-phenyl	0.031 ± 0.003	>10	>10
12f	H	3-CF_3-phenyl	0.013 ± 0.002	>10	0.88 ± 0.10
12g	H	2-CF_3-phenyl	0.012 ± 0.003	>10	0.88 ± 0.20
12h	H	4-F-phenyl	0.037 ± 0.003	>10	6.8 ± 1.0
12i	H	3-F-phenyl	0.014 ± 0.002	>10	0.49 ± 0.20
12j	H	2-F-phenyl	0.015 ± 0.0001	>10	0.77 ± 0.10
12k	H	4-Cl-phenyl	0.012 ± 0.001	>10	0.64 ± 0.10
12l	H	3-Cl-phenyl	0.011 ± 0.002	>10	0.59 ± 0.05
12m	H	4-Br-phenyl	0.010 ± 0.000	7.0 ± 2.0	NT[b]
12n	H	3-Br-phenyl	0.011 ± 0.0002	>10	1.2 ± 0.3
12o	H	2-Br-phenyl	0.008 ± 0.0003	>10	1.1 ± 0.2
12p	H	4-NO_2-phenyl	0.012 ± 0.002	>10	3.4 ± 0.4
12q	H	4-OH-phenyl	0.011 ± 0.0004	>10	1.6 ± 0.2
12r	H	4-OMe-phenyl	0.012 ± 0.0003	>10	3.6 ± 0.7
12s	H	3-OMe-phenyl	0.013 ± 0.0003	>10	2.7 ± 0.5
12t	H	2-OMe-phenyl	0.017 ± 0.002	>10	8.4 ± 2.0
12u	H	naphthyl	0.007 ± 0.0004	~10	0.79 ± 0.20
13a	H	biphenyl	0.09 ± 0.00	3.2 ± 1.2	NT[b]
13b	H	4'-Me-biphenyl	0.006 ± 0.0003	7.0 ± 4.9	>1.0[c]
13c	H	4'-CF_3-biphenyl	0.039 ± 0.003	8.4 ± 0.6	>1.0[c]

Table 1 (*continued*)

Compd	R^1	R^2	RT RNase H IC_{50}[a] (µM)	RT pol IC_{50}[a] (µM)	INST IC_{50}[a] (µM)
13d	H		0.008 ± 0.0001	>10	>100
13e	H		0.006 ± 0.0005	>10	>1.0[c]
13f	H		0.005 ± 0.0004	~10	>1.0[c]
13g	H		0.007 ± 0.001	>10	>1.0[c]
13h	H		0.004 ± 0.0001	>10	0.17 ± 0.04
13i	H		0.006 ± 0.0002	~10	>100
13j	H		0.005 ± 0.0004	~10	>1.0[c]
13k	H		0.004 ± 0.0001	~10	0.33 ± 0.06
13l	H		0.006 ± 0.0004	>10	>100
13m	H		0.005 ± 0.0003	>10	>10
13n	H		0.004 ± 0.0001	6.8 ± 5.0	>0.14[c]
13o	H		0.007 ± 0.002	~10	>0.14[c]
13p	H		0.007 ± 0.0006	7.7 ± 0.6	>1.0[c]
13q	H		0.005 ± 0.0005	9.9 ± 0.2	>0.14[c]
13r	H		0.006 ± 0.0003	9.6 ± 0.9	0.24 ± 0.09
13s	H		0.005 ± 0.0005	7.8 ± 0.04	>1.0[c]
13t	H		0.005 ± 0.002	5.6 ± 1.0	>1.0[c]
13u	H		0.013 ± 0.003	>10	>100
13v	H		0.012 ± 0.001	>10	>100
20a	Br		0.070 ± 0.008	5.0 ± 0.8	NT[b]
20b	I		0.12 ± 0.00	0.46 ± 0.09	NT[b]
10j	R = *meta*-OMe		0.15	7.3	>100
7	–		0.70	0.85	NT[b]
RAL	–		>10	NT[b]	0.65 ± 0.14
DTG	–		>10	NT[b]	0.068 ± 0.010

[a] Concentration of a compound inhibiting the enzymatic function by 50%, expressed as the mean ± standard deviation from at least two independent experiments.

[b] NT = not tested.

[c] Compound did not behave well in the assay and accurate measurement of IC_{50} was not allowed.

Table 2
Antiviral activity of subtypes **12** and **13** analogues against HIV-1.

Compd	Antiviral Profile		Biochemical Inhibition[c]		
	EC$_{50}$[a] (μM)	CC$_{50}$[b] (μM)	RNase H IC$_{50}$ (μM)	INST IC$_{50}$ (μM)	SI[d]
12a	11 ± 0.6	>100	0.016 ± 0.002	1.1 ± 0.3	69
12b	>20	>100	0.033 ± 0.003	2.8 ± 0.6	85
12c	11 ± 0.8	>100	0.010 ± 0.0003	1.3 ± 0.2	1.3 × 10^2
12d	6.2 ± 0.2	>100	0.010 ± 0.002	0.75 ± 0.09	75
12e	>20	>100	0.031 ± 0.003	>10	>3.2 × 102
12f	6.2 ± 0.8	>100	0.013 ± 0.002	0.88 ± 0.10	68
12g	6.6 ± 1	>100	0.012 ± 0.003	0.88 ± 0.20	73
12h	>20	>100	0.037 ± 0.003	6.8 ± 1.0	1.8 × 10^2
12i	9.1 ± 0.7	>100	0.014 ± 0.002	0.49 ± 0.20	35
12j	4.7 ± 0.9	>100	0.015 ± 0.0001	0.77 ± 0.10	51
12k	>20	>100	0.012 ± 0.001	0.64 ± 0.10	53
12l	6.3 ± 1	>100	0.011 ± 0.002	0.59 ± 0.05	54
12n	8.2 ± 0.2	>100	0.011 ± 0.002	1.2 ± 0.3	1.1 × 10^2
12o	6.5 ± 0.3	>100	0.0080 ± 0.0003	1.1 ± 0.2	1.4 × 10^2
12p	>20	>100	0.012 ± 0.002	3.4 ± 0.4	2.8 × 10^2
12q	>20	>100	0.011 ± 0.0004	1.6 ± 0.2	1.5 × 10^2
12r	>20	>100	0.012 ± 0.0003	3.6 ± 0.7	3.0 × 10^2
12s	16 ± 2	>100	0.013 ± 0.0003	2.7 ± 0.5	2.1 × 10^2
12t	9.0 ± 1	>100	0.017 ± 0.002	8.4 ± 2.0	4.9 × 10^2
12u	6.3 ± 0.9	>100	0.007 ± 0.0004	0.79 ± 0.20	1.1 × 10^2
13b	7.5 ± 1	>100	0.006 ± 0.0003	>1.0	>1.7 × 10^2
13c	12 ± 2	>100	0.039 ± 0.003	>1.0	26
13d	>20	>100	0.008 ± 0.0001	>100	>1.3 × 10^4
13e	12 ± 1	>100	0.006 ± 0.0005	>1.0	>1.7 × 10^2
13f	7.2 ± 1	>100	0.005 ± 0.0004	>1.0	>2.0 × 10^2
13g	16 ± 2	>100	0.007 ± 0.001	>1.0	>1.4 × 10^2
13h	10 ± 0.2	>100	0.004 ± 0.0001	0.17 ± 0.04	43
13i	10 ± 0.2	>100	0.006 ± 0.0002	>100	>1.7 × 10^4
13j	7.7 ± 0.6	>100	0.005 ± 0.0004	>1.0	>2.0 × 10^2
13k	>20	>100	0.004 ± 0.0001	0.33 ± 0.06	83
13l	17 ± 0.3	>100	0.006 ± 0.0004	>100	>1.7 × 10^4
13m	18 ± 0.6	>100	0.005 ± 0.0003	>10	>2.0 × 10^3
13n	8.0 ± 0.6	>100	0.004 ± 0.0001	>0.14	>35
13o	11 ± 0.3	>100	0.007 ± 0.002	>0.14	>20
13p	8.3 ± 0.5	>100	0.007 ± 0.0006	>1.0	>1.4 × 10^2
13q	5.0 ± 0.9	>100	0.005 ± 0.0005	>0.14	>28
13r	6.5 ± 2	>100	0.006 ± 0.0003	0.24 ± 0.09	40
13s	10 ± 2	>100	0.005 ± 0.0005	>1.0	>2.0 × 10^2
13t	11 ± 2	>100	0.005 ± 0.002	>1.0	>2.0 × 10^2
13u	7.0 ± 0.6	>100	0.013 ± 0.003	>100	>7.7 × 10^3
13v	11 ± 1	>100	0.012 ± 0.001	>100	>8.3 × 10^3
10j	>25	>25	0.15	>100	>6.7 × 10^2
RAL	0.03	−	>10	0.65 ± 0.14	<0.065
DTG	0.02	−	>10	0.068 ± 0.010	<0.0068

[a] Concentration of a compound inhibiting HIV-1 replication by 50%, expressed as the mean ± standard deviation from at least two independent experiments.
[b] Concentration of a compound causing 50% cytotoxicity, expressed as the mean ± standard deviation from at least three independent experiments.
[c] Significant RT pol inhibition was not observed against any of these compounds.
[d] Selectivity index, defined as INST IC$_{50}$/RNase H IC$_{50}$.

Table 3
PAMPA permeability for selected analogues of subtypes **12** and **13**.

Compd	EC$_{50}$ (μM)	RNase H IC$_{50}$ (μM)	INST IC$_{50}$ (μM)	P$_e$ (10^{-6} cm/s)
12b	>20	0.033 ± 0.003	2.8 ± 0.6	0.92
12k	>20	0.012 ± 0.001	0.64 ± 0.10	0.35
12p	>20	0.012 ± 0.002	3.4 ± 0.4	0.032
13h	>20	0.0040 ± 0.0001	0.17 ± 0.04	0.039
13k	>20	0.0040 ± 0.0001	0.33 ± 0.06	0.90

conducted also with analogue **13q** using a PFV intasome model (PDB code: 3S3M [29]). Significantly, **13q** fits perfectly into the IN binding site through the anchoring interaction between the HPD core (the 2-C=O-3-OH-4-C=O chelating triad) and the two metal cofactors (Mg^{2+}) which are coordinated to the active site acidic residues D128, D185 and E221. The binding to metal cofactors allows the placement of the thio-biphenyl group into the protein-DNA interfacial hydrophobic pocket to engage in a few molecular interactions: i) π-alkyl interaction between the biphenyl group of **13q** with the P214 ii) π-π stacking of the central uracil ring with the terminal 3′-deoxyadenosine A17 and iii) π-sulfur interaction between the thiol group within **13q** and terminal 3′-deoxyadenosine A17.

3. Conclusions

New HPD subtypes featuring a C-6 arylthio moiety were designed and synthesized as inhibitors of the HIV RT-associated RNase H domain. Biochemical assays against RT RNase H, RT pol, and INST revealed that both the 6-phenylthio HPD subtype **12** and the 6-biphenylthio HPD subtype **13** inhibited RNase H in low nM range without significant inhibition of RT pol. Many analogues also inhibited INST, though the level of inhibition (low to sub micromolar range) was much lower than that observed for RNase H inhibition. Consistent antiviral activity against HIV-1 was also observed with most analogues in low μM range without cytotoxicity at concentrations up to 100 μM. The combined biochemical
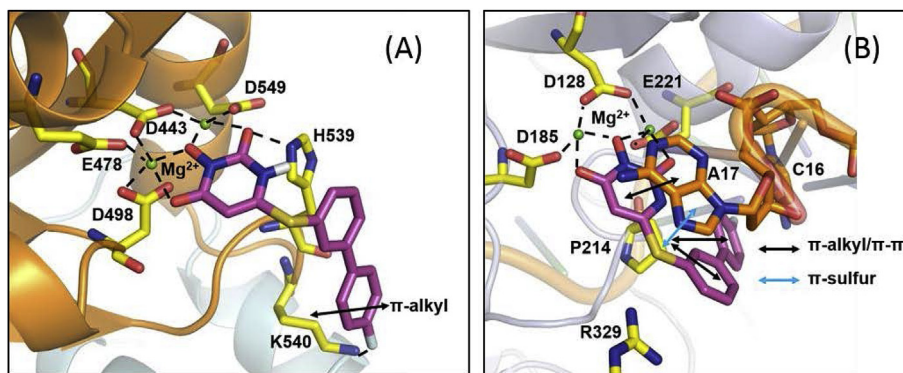
Fig. 2. Molecular modeling of compound **13q** within the HIV RNase H and PFV integrase active site. (A) Predicted binding mode of **13q** (magenta) within the active site of RNase H (PDB code: 5J1E [20]). The p66 and p51 subunits of RT are shown in orange and gray cartoon, respectively. (B) The PFV intasome catalytic site (PDB code: 3S3M [29]). Active site residues are highlighted in yellow sticks with metal ions (Mg^{2+}) as green spheres. Chelating and H-bond interactions are depicted as black dotted lines. The π-alkyl or π-π and π-sulfur interactions are shown in black and blue double-headed arrows respectively. Viral DNA in Figure B is shown in orange cartoon and sticks. (For interpretation of the references to colour in this figure legend, the reader is referred to the Web version of this article.)

and antiviral profiles of the current 6-arylthio HPD subtypes represent an exciting advancement in research targeting HIV RNase H.

4. Experimental

4.1. Chemistry

General Procedures. All commercial chemicals were used as supplied unless otherwise indicated. Microwave synthesis was performed with a Biotage Initiator Microwave Synthesizer. Flash chromatography was performed on a Teledyne Combiflash RF-200 with RediSep columns (silica) and indicated mobile phase. All moisture sensitive reactions were performed under an inert atmosphere of ultra-pure argon with oven-dried glassware. ^{1}H and ^{13}C NMR spectra were recorded on a Varian 600 MHz or Bruker 400 spectrometer. Mass data were acquired using an Agilent 6230 TOF LC/MS spectrometer. All NMR and mass spectrometers are located in the shared instrument rooms at the Center for Drug Design, University of Minnesota. Analysis of sample purity was performed on a Agilent Varian Prepstar SD-1 HPLC system located in our own lab with a Phenomenex Gemini, 5 μm C18 column (250 mm × 4.6 mm). HPLC conditions: solvent A: H$_2$O with 0.1% TFA; solvent B: MeCN; flow rate 1.0 mL/min; compounds were eluted with a gradient of 20% MeCN/H$_2$O with 0.1% TFA to 100% MeCN for 20 min. All tested compounds have a purity ≥97%.

4.1.1. General Procedure for Synthesis of 12

To a microwave reaction vessel were added compound **18** (30 mg) and TFA (2–3 mL). The reaction vessel was irradiated at 120 °C for the appropriate time. The reaction was monitored by TLC and MS. The reaction mixture was then concentrated and the crude product was purified by Combiflash (MeOH/DCM, 1%–5%) or trituration with MeOH, ethyl acetate, and DCM yielded pure compounds.

4.1.2. 3-Hydroxy-6-(phenylthio)pyrimidine-2,4(1H,3H)-dione (12a)

Yield 79%. White solid, m. p. 220–222 °C; ^{1}H NMR (600 MHz, DMSO-d_6) δ 11.98 (s, 1H), 10.35 (s, 1H), 7.62 (d, $J = 7.4$ Hz, 2H), 7.68 (t, $J = 7.4$ Hz, 1H), 7.54 (t, $J = 7.4$ Hz, 2H), 4.66 (s, 1H); ^{13}C NMR (150 MHz, DMSO-d_6) δ 159.2, 153.7, 149.5, 135.9, 131.3, 130.8, 126.8, 96.1. HRMS-ESI(−) m/z calcd for C$_{10}$H$_8$N$_2$O$_3$S [M − H]$^-$ 235.0183, found 235.0189.

4.1.3. 3-Hydroxy-6-(p-tolylthio)pyrimidine-2,4(1H,3H)-dione (12b)

Yield 60%. White solid, m. p. 205–207 °C; ^{1}H NMR (600 MHz, DMSO-d_6) δ 11.92 (s, 1H), 7.50 (d, $J = 8.1$ Hz, 2H), 7.36 (d, $J = 7.9$ Hz, 2H), 4.60 (s, 1H), 2.37 (s, 3H); ^{13}C NMR (150 MHz, DMSO-d_6) δ 160.7, 150.4, 149.9, 141.5, 129.8, 128.8, 127.3, 97.3, 21.3; HRMS-ESI(−) m/z calcd for C$_{11}$H$_{10}$N$_2$O$_3$S [M − H]$^-$ 249.0339, found 249.0334.

4.1.4. 6-((4-Ethylphenyl)thio)-3-hydroxypyrimidine-2,4(1H,3H)-dione (12c)

Yield 65%. White solid, m. p. 165–167 °C; ^{1}H NMR (600 MHz, DMSO-d_6) δ 11.95 (s, 1H), 10.34 (s, 1H), 7.53 (d, $J = 8.0$ Hz, 2H), 7.39 (d, $J = 8.0$ Hz, 2H), 4.61 (s, 1H), 2.66 (q, $J = 7.6$ Hz, 2H), 1.19 (t, $J = 7.6$ Hz, 3H); ^{13}C NMR (150 MHz, DMSO-d_6) δ 159.2, 154.4, 149.5, 147.6, 136.1, 130.2, 123.4, 95.6, 28.3, 15.7; HRMS-ESI(−) m/z calcd for C$_{12}$H$_{12}$N$_2$O$_3$S [M − H]$^-$ 263.0496, found 263.0497.

4.1.5. 6-((2-Ethylphenyl)thio)-3-hydroxypyrimidine-2,4(1H,3H)-dione (12d)

Yield 69%. White solid, m. p. 168–170 °C; ^{1}H NMR (600 MHz, DMSO-d_6) δ 11.99 (s, 1H), 10.34 (s, 1H), 7.58–7.53 (m, 2H), 7.49 (d, $J = 7.2$ Hz, 1H), 7.36 (t, $J = 7.2$ Hz, 1H), 4.44 (s, 1H), 2.72 (q, $J = 7.2$ Hz, 2H), 1.13 (t, $J = 7.2$ Hz, 3H); ^{13}C NMR (150 MHz, DMSO-d_6) δ 159.2, 153.9, 149.5, 148.7, 137.6, 132.2, 130.6, 128.3, 125.4, 95.1, 27.1, 15.9; HRMS-ESI(−) m/z calcd for C$_{12}$H$_{12}$N$_2$O$_3$S [M − H]$^-$ 263.0496, found 263.0499.

4.1.6. 3-Hydroxy-6-((4-(trifluoromethyl)phenyl)thio)pyrimidine-2,4(1H,3H)-dione (12e)

Yield 71%. White solid, m. p. 210–212 °C; ^{1}H NMR (600 MHz, DMSO-d_6) δ 11.96 (s, 1H), 10.41 (s, 1H), 7.85 (d, $J = 8.2$ Hz, 2H), 7.78 (d, $J = 8.2$ Hz, 2H), 5.14 (s, 1H); ^{13}C NMR (150 MHz, DMSO-d_6) δ 159.3, 149.9, 149.7, 134.6, 134.0, 130.3 (q, $J_{CF} = 32.2$ Hz), 127.2 (q, $J_{CF} = 3.6$ Hz), 124.3 (q, $J_{CF} = 272.4$ Hz), 99.7; HRMS-ESI(−) m/z calcd for C$_{11}$H$_7$F$_3$N$_2$O$_3$S [M − H]$^-$ 303.0057, found 303.0063.

4.1.7. 3-Hydroxy-6-((3-(trifluoromethyl)phenyl)thio)pyrimidine-2,4(1H,3H)-dione (12f)

Yield 79%. White solid, m. p. 170–172 °C; ^{1}H NMR (600 MHz, DMSO-d_6) δ 11.99 (s, 1H), 10.41 (s, 1H), 7.99 (s, 1H), 7.92–7.91 (m, 2H), 7.75 (t, $J = 7.8$ Hz, 1H), 4.94 (s, 1H); ^{13}C NMR (150 MHz, DMSO-d_6) δ 159.3, 151.3, 149.6, 139.1, 131.7, 131.4 (q, $J_{CF} = 3.8$ Hz), 131.1 (q, $J_{CF} = 32.3$ Hz), 129.5, 127.5 (q, $J_{CF} = 3.7$ Hz), 124.0 (q, $J_{CF} = 272.8$ Hz), 98.3; HRMS-ESI(−) m/z calcd for C$_{11}$H$_7$F$_3$N$_2$O$_3$S [M − H]$^-$ 303.0057, found 303.0061.

4.1.8. 3-Hydroxy-6-((2-(trifluoromethyl)phenyl)thio)pyrimidine-2,4(1H,3H)-dione (12g)

Yield 81%. White solid, m. p. 208–210 °C; 1H NMR (600 MHz, DMSO-d_6) δ 12.09 (s, 1H), 10.40 (s, 1H), 7.98 (d, $J = 7.7$ Hz, 1H), 7.89 (d, $J = 7.7$ Hz, 1H), 7.83 (t, $J = 7.7$ Hz, 1H), 7.79 (t, $J = 7.7$ Hz, 1H), 4.63 (s, 1H); 13C NMR (150 MHz, DMSO-d_6) δ 159.2, 152.1, 149.4, 139.5, 134.7 (q, $J_{CF} = 3.7$ Hz), 132.3 (q, $J_{CF} = 29.9$ Hz), 132.1 (q, $J_{CF} = 3.7$ Hz), 128.5 (q, $J_{CF} = 5.4$ Hz), 125.5, 123.6 (q, $J_{CF} = 273.9$ Hz), 97.4; HRMS-ESI(−) m/z calcd for $C_{11}H_7F_3N_2O_3S$ [M − H]$^-$ 303.0057, found 303.0059.

4.1.9. 6-((4-Fluorophenyl)thio)-3-hydroxypyrimidine-2,4(1H,3H)-dione (12h)

Yield 77%. White solid, m. p. 185–187 °C; 1H NMR (600 MHz, DMSO-d_6) δ 11.95 (s, 1H), 10.34 (s, 1H), 7.70 (dd, $J = 8.6, 5.3$ Hz, 2H), 7.39 (t, $J = 8.7$ Hz, 2H), 4.68 (s, 1H); 13C NMR (100 MHz, DMSO-d_6) δ 164.1 (d, $J_{CF} = 249.6$ Hz), 159.2, 153.7, 149.5, 138.6 (d, $J_{CF} = 8.9$ Hz), 122.5, 118.0 (d, $J_{CF} = 22.2$ Hz), 96.1; HRMS-ESI(−) m/z calcd for $C_{10}H_7FN_2O_3S$ [M − H]$^-$ 253.0089, found 253.0089.

4.1.10. 6-((3-Fluorophenyl)thio)-3-hydroxypyrimidine-2,4(1H,3H)-dione (12i)

Yield 69%. White solid, m. p. 195–197 °C; 1H NMR (600 MHz, DMSO-d_6) δ 11.98 (s, 1H), 10.41 (s, 1H), 7.60–7.55 (m, 2H), 7.46 (d, $J = 7.7$ Hz, 1H), 7.42 (t, $J = 8.6$ Hz, 1H), 4.88 (s, 1H); 13C NMR (150 MHz, DMSO-d_6) δ 162.7 (d, $J_{CF} = 248.0$ Hz), 159.3, 151.9, 149.6, 132.5 (d, $J_{CF} = 8.4$ Hz), 131.4 (d, $J_{CF} = 2.9$ Hz), 129.4 (d, $J_{CF} = 8.3$ Hz), 121.9 (d, $J_{CF} = 22.7$ Hz), 118.1 (d, $J_{CF} = 20.9$ Hz), 97.6; HRMS-ESI(−) m/z calcd for $C_{10}H_7FN_2O_3S$ [M − H]$^-$ 253.0089, found 253.0086.

4.1.11. 6-((2-Fluorophenyl)thio)-3-hydroxypyrimidine-2,4(1H,3H)-dione (12j)

Yield 68%. White solid, m. p. 130–132 °C; 1H NMR (600 MHz, DMSO-d_6) δ 12.05 (s, 1H), 10.40 (s, 1H), 7.71–7.65 (m, 2H), 7.47 (t, $J = 8.8$ Hz, 1H), 7.37 (t, $J = 7.6$ Hz, 1H), 4.71 (s, 1H); 13C NMR (150 MHz, DMSO-d_6) δ 162.2 (d, $J_{CF} = 248.8$ Hz), 159.1, 151.5, 149.5, 137.9, 134.5 (d, $J_{CF} = 8.4$ Hz), 126.6 (d, $J_{CF} = 3.7$ Hz), 117.4 (d, $J_{CF} = 22.1$ Hz), 114.0 (d, $J_{CF} = 17.9$ Hz), 96.1; HRMS-ESI(−) m/z calcd for $C_{10}H_7FN_2O_3S$ [M − H]$^-$ 253.0089, found 253.0093.

4.1.12. 6-((4-Chlorophenyl)thio)-3-hydroxypyrimidine-2,4(1H,3H)-dione (12k)

Yield 89%. White solid, m. p. 198–200 °C; 1H NMR (600 MHz, DMSO-d_6) δ 11.98 (s, 1H), 10.40 (s, 1H), 7.64 (d, $J = 8.5$ Hz, 2H), 7.60 (d, $J = 8.5$ Hz, 2H), 4.79 (s, 1H); 13C NMR (150 MHz, DMSO-d_6) δ 159.2, 152.7, 149.5, 137.3, 136.2, 130.8, 126.1, 96.9; HRMS-ESI(−) m/z calcd for $C_{10}H_7ClN_2O_3S$ [M − H]$^-$ 268.9793, found 268.9797.

4.1.13. 6-((3-Chlorophenyl)thio)-3-hydroxypyrimidine-2,4(1H,3H)-dione (12l)

Yield 90%. White solid, m. p. 150–152 °C; 1H NMR (600 MHz, DMSO-d_6) δ 11.96 (s, 1H), 10.40 (s, 1H), 7.73 (s, 1H), 7.62 (d, $J = 7.8$ Hz, 1H), 7.59–7.53 (m, 2H), 4.90 (s, 1H); 13C NMR (150 MHz, DMSO-d_6) δ 159.3, 151.7, 149.6, 134.7, 134.4, 133.8, 132.2, 130.9, 129.7, 97.9; HRMS-ESI(−) m/z calcd for $C_{10}H_7ClN_2O_3S$ [M − H]$^-$ 268.9793, found 268.9795.

4.1.14. 6-((4-Bromophenyl)thio)-3-hydroxypyrimidine-2,4(1H,3H)-dione (12m)

Yield 68%. 1H NMR (600 MHz, CD$_3$OD) δ 7.97 (d, $J = 7.8$ Hz, 2H), 7.80 (d, $J = 7.8$ Hz, 2H), 5.26 (s, 1H); 13C NMR (150 MHz, DMSO-d_6) δ 162.7, 155.7, 151.2, 37.6, 133.6, 126.0, 125.0, 97.1; HRMS-ESI(−) m/z calcd. for $C_{10}H_7BrN_2O_3S$ [M − H]$^-$ 312.9287, found 312.9289.

4.1.15. 6-((3-Bromophenyl)thio)-3-hydroxypyrimidine-2,4(1H,3H)-dione (12n)

Yield 73%. White solid, m. p. 152–154 °C; 1H NMR (600 MHz, DMSO-d_6) δ 11.94 (s, 1H), 10.39 (s, 1H), 7.85 (s, 1H), 7.75 (d, $J = 7.8$ Hz, 1H), 7.62 (d, $J = 7.8$ Hz, 1H), 7.47 (t, $J = 7.8$ Hz, 1H), 4.91 (s, 1H); 13C NMR (150 MHz, DMSO-d_6) δ 159.3, 151.8, 149.6, 137.1, 134.2, 133.8, 132.5, 129.9, 123.1, 97.9; HRMS-ESI(−) m/z calcd for $C_{10}H_7BrN_2O_3S$ [M − H]$^-$ 312.9288, found 312.9286.

4.1.16. 6-((2-Bromophenyl)thio)-3-hydroxypyrimidine-2,4(1H,3H)-dione (12o)

Yield 66%. White solid, m. p. 205–207 °C; 1H NMR (600 MHz, DMSO-d_6) δ 12.01 (s, 1H), 10.39 (s, 1H), 7.87 (d, $J = 7.9$ Hz, 1H), 7.75 (d, $J = 7.9$ Hz, 1H), 7.53 (t, $J = 7.9$ Hz, 1H), 7.48 (t, $J = 7.9$ Hz, 1H), 4.75 (s, 1H); 13C NMR (150 MHz, DMSO-d_6) δ 159.2, 150.8, 149.6, 137.4, 134.6, 133.0, 129.9, 129.0, 128.8, 97.3; HRMS-ESI(−) m/z calcd for $C_{10}H_7BrN_2O_3S$ [M − H]$^-$ 312.9288, found 312.9282.

4.1.17. 3-Hydroxy-6-((4-nitrophenyl)thio)pyrimidine-2,4(1H,3H)-dione (12p)

Yield 84%. Pale yellow solid, m. p. 238–240 °C; 1H NMR (600 MHz, DMSO-d_6) δ 12.00 (s, 1H), 10.51 (s, 1H), 8.26 (d, $J = 8.6$ Hz, 2H), 7.78 (d, $J = 8.4$ Hz, 2H), 5.43 (s, 1H); 13C NMR (150 MHz, DMSO-d_6) δ 159.4, 149.7, 147.9, 147.7, 138.3, 133.4, 125.1, 102.0; HRMS-ESI(−) m/z calcd for $C_{10}H_7N_3O_5S$ [M − H]$^-$ 280.0034, found 280.0039.

4.1.18. 3-Hydroxy-6-((4-hydroxyphenyl)thio)pyrimidine-2,4(1H,3H)-dione (12q)

Yield 79%. White solid, m. p. 190–192 °C; 1H NMR (600 MHz, DMSO-d_6) δ 11.87 (s, 1H), 10.28 (s, 1H), 7.41 (d, $J = 8.2$ Hz, 2H), 6.90 (d, $J = 8.2$ Hz, 2H), 4.55 (s, 1H); 13C NMR (100 MHz, DMSO-d_6) δ 160.5, 159.3, 155.8, 149.5, 138.3, 117.7, 114.3, 94.7; HRMS-ESI(−) m/z calcd for $C_{10}H_8N_2O_4S$ [M − H]$^-$ 251.0132, found 251.0135.

4.1.19. 3-Hydroxy-6-((4-methoxyphenyl)thio)pyrimidine-2,4(1H,3H)-dione (12r)

Yield 69%. White solid, m. p. 190–192 °C; 1H NMR (600 MHz, DMSO-d_6) δ 11.94 (s, 1H), 10.34 (s, 1H), 7.55 (d, $J = 8.2$ Hz, 2H), 7.10 (d, $J = 8.2$ Hz, 2H), 4.54 (s, 1H), 3.82 (s, 3H); 13C NMR (150 MHz, DMSO-d_6) δ 161.8, 159.2, 155.3, 149.5, 138.1, 116.5, 116.4, 94.9, 56.0; HRMS-ESI(−) m/z calcd for $C_{11}H_{10}N_2O_4S$ [M − H]$^-$ 265.0289, found 265.0291.

4.1.20. 3-Hydroxy-6-((3-methoxyphenyl)thio)pyrimidine-2,4(1H,3H)-dione (12s)

Yield 59%. White solid, m. p. 192–194 °C; 1H NMR (600 MHz, DMSO-d_6) δ 11.93 (s, 1H), 10.34 (s, 1H), 7.45 (t, $J = 8.2$ Hz, 1H), 7.18–7.17 (m, 2H), 7.15–7.13 (m, 1H), 4.77 (s, 1H), 3.78 (s, 3H); 13C NMR (150 MHz, DMSO-d_6) δ 160.6, 159.3, 153.4, 149.5, 131.6, 127.82, 127.75, 120.7, 117.1, 96.3, 56.0; HRMS-ESI(−) m/z calcd for $C_{11}H_{10}N_2O_4S$ [M − H]$^-$ 265.0289, found 265.0292.

4.1.21. 3-Hydroxy-6-((2-methoxyphenyl)thio)pyrimidine-2,4(1H,3H)-dione (12t)

Yield 61%. White solid, m. p. 148–150 °C; 1H NMR (600 MHz, CDCl$_3$) δ 7.53–7.50 (m, 2H), 7.04–7.01 (m, 2H), 5.45 (s, 1H), 3.89 (s, 3H); 13C NMR (150 MHz, CDCl$_3$) δ 159.9, 158.7, 151.9, 147.0, 137.9, 133.9, 122.1, 112.5, 112.4, 95.9, 56.3; HRMS-ESI(−) m/z calcd for $C_{11}H_{10}N_2O_4S$ [M − H]$^-$ 265.0289, found 265.0294.

4.1.22. 3-Hydroxy-6-(naphthalen-1-ylthio)pyrimidine-2,4(1H,3H)-dione (12u)

Yield: 70%. White solid, m. p. 225–227 °C; 1H NMR (600 MHz, DMSO-d_6) δ 12.11 (s, 1H), 10.31 (s, 1H), 8.23–8.19 (m, 2H), 8.10 (d,

$J = 7.9$ Hz, 1H), 7.99 (d, $J = 7.0$ Hz, 1H), 7.69 (t, $J = 8.0$ Hz, 1H), 7.67–7.64 (m, 2H), 4.33 (s, 1H). ^{13}C NMR (150 MHz, DMSO-d_6) δ 159.1, 153.2, 149.51, 137.1, 134.5, 133.7, 132.8, 129.5, 128.8, 127.6, 126.9, 125.1, 123.5, 95.7; HRMS-ESI(−) m/z calcd for $C_{14}H_{10}N_2O_3S$ [M − H]$^-$ 285.0339, found 285.0339.

4.1.23. General Procedure for Synthesis of 20

These analogues were synthesized following the synthetic procedure of **12** except that compounds **19** were used as the starting materials.

4.1.24. 5-Bromo-6-((4-bromophenyl)thio)-3-hydroxypyrimidine-2,4(1H,3H)-dione (20a)

Yield 53%. ^{1}H NMR (600 MHz, CD$_3$OD) δ 7.53 (d, $J = 7.8$ Hz, 2H), 7.35 (d, $J = 7.8$ Hz, 2H); HRMS-ESI(−) m/z calcd. for $C_{10}H_6Br_2N_2O_3S$ [M − H]$^-$ 390.8392, found 390.8390.

4.1.25. 6-((4-Bromophenyl)thio)-3-hydroxy-5-iodopyrimidine-2,4(1H,3H)-dione (20b)

Yield 50%. ^{1}H NMR (600 MHz, DMSO-d_6) δ 12.04 (s, 1H), 10.84 (s, 1H), 7.89 (d, $J = 7.8$ Hz, 2H), 7.56 (d, $J = 7.8$ Hz, 2H); ^{13}C NMR (150 MHz, DMSO-d_6) δ 161.3, 152.1, 151.1, 134.0, 133.0, 129.9, 122.6, 77.9; HRMS-ESI(−) m/z calcd. for $C_{10}H_6BrIN_2O_3S$ [M − H]$^-$ 438.8253, found 438.8356.

General Procedure for Synthesis of 13. These analogues were synthesized following the synthetic procedure of **12** except that compounds **21** were used as the starting materials.

4.1.26. 6-([1,1'-biphenyl]-4-ylthio)-3-hydroxypyrimidine-2,4(1H,3H)-dione (13a)

Yield 63%. White solid, m. p. > 250 °C; ^{1}H NMR (600 MHz, DMSO-d_6) δ 12.05 (s, 1H), 10.44, (s, 1H), 7.91 (d, $J = 6.6$ Hz, 2H), 7.82 (d, $J = 7.2$ Hz, 2H), 7.78 (d, $J = 7.8$ Hz, 2H), 7.72 (t, $J = 9.0$ Hz, 2H), 7.58–7.50 (m, 1H), 4.78 (s, 1H); ^{13}C NMR (150 MHz, DMSO-d_6) δ 162.7, 156.8, 151.3, 142.8, 139.1, 136.4, 129.6, 128.9, 128.7, 127.4, 125.5, 96.5; HRMS-ESI(−) m/z calcd. for $C_{16}H_{12}N_2O_3S$ [M − H]$^-$ 314.0495, found 314.0492.

4.1.27. 3-Hydroxy-6-((4'-methyl-[1,1'-biphenyl]-4-yl)thio) pyrimidine-2,4(1H,3H)-dione (13b)

Yield 60%. White solid, m. p. 238–240 °C; ^{1}H NMR (600 MHz, DMSO-d_6) δ 11.99 (s, 1H), 10.38 (s, 1H), 7.81 (d, $J = 8.3$ Hz, 2H), 7.67 (d, $J = 8.2$ Hz, 2H), 7.63 (d, $J = 8.0$ Hz, 2H), 7.30 (d, $J = 7.9$ Hz, 2H), 4.77 (s, 1H), 2.34 (s, 3H); ^{13}C NMR (150 MHz, DMSO-d_6) δ 159.2, 153.6, 149.5, 142.8, 138.2, 136.3, 136.2, 130.1, 128.6, 127.2, 125.3, 96.2, 21.2; HRMS-ESI(−) m/z calcd for $C_{17}H_{14}N_2O_3S$ [M − H]$^-$ 325.0652, found 325.0659.

4.1.28. 3-Hydroxy-6-((4'-(trifluoromethyl)-[1,1'-biphenyl]-4-yl) thio)pyrimidine-2,4(1H,3H)-dione (13c)

Yield 68%. White solid, m. p. 240–242 °C; ^{1}H NMR (600 MHz, DMSO-d_6) δ 11.99 (s, 1H), 10.38 (s, 1H), 7.96 (d, $J = 8.0$ Hz, 2H), 7.90 (d, $J = 8.2$ Hz, 2H), 7.84 (d, $J = 8.1$ Hz, 2H), 7.74 (d, $J = 8.1$ Hz, 2H), 4.86 (s, 1H); HRMS-ESI(−) m/z calcd for $C_{17}H_{11}F_3N_2O_3S$ [M − H]$^-$ 379.0370, found 379.0371.

4.1.29. 3-Hydroxy-6-((3'-(trifluoromethyl)-[1,1'-biphenyl]-4-yl) thio)pyrimidine-2,4(1H,3H)-dione (13d)

Yield 61%. White solid, m. p. 180–182 °C; ^{1}H NMR (600 MHz, DMSO-d_6) δ 11.98 (s, 1H), 10.37 (s, 1H), 8.06–8.05 (m, 2H), 7.92 (d, $J = 8.3$ Hz, 2H), 7.78 (d, $J = 7.7$ Hz, 1H), 7.74–7.72 (m, 3H), 4.84 (s, 1H); HRMS-ESI(−) m/z calcd for $C_{17}H_{11}F_3N_2O_3S$ [M − H]$^-$ 379.0370, found 379.0372.

4.1.30. 6-((4'-fluoro-[1,1'-biphenyl]-4-yl)thio)-3-hydroxypyrimidine-2,4(1H,3H)-dione (13e)

Yield 60%. White solid, m. p. 240–242 °C; ^{1}H NMR (600 MHz, DMSO-d_6) δ 11.97 (s, 1H), 10.35 (s, 1H), 7.82–7.78 (m, 4H), 7.69 (d, $J = 8.2$ Hz, 2H), 7.32 (t, $J = 8.8$ Hz, 2H), 4.80 (s, 1H); ^{13}C NMR (150 MHz, DMSO-d_6) δ 162.8 (d, $J_{CF} = 245.4$ Hz), 159.2, 153.4, 149.5, 141.8, 136.3, 135.6 (d, $J_{CF} = 3.1$ Hz), 129.5 (d, $J_{CF} = 8.3$ Hz), 128.8, 125.9, 116.4 (d, $J_{CF} = 21.5$ Hz), 96.4; HRMS-ESI(−) m/z calcd for $C_{16}H_{11}FN_2O_3S$ [M − H]$^-$ 329.0402, found 329.0400.

4.1.31. 6-((3'-fluoro-[1,1'-biphenyl]-4-yl)thio)-3-hydroxypyrimidine-2,4(1H,3H)-dione (13f)

Yield 79%. White solid, m. p. 238–240 °C; ^{1}H NMR (600 MHz, DMSO-d_6) δ 11.98 (s, 1H), 10.36 (s, 1H), 7.87 (d, $J = 8.3$ Hz, 2H), 7.70 (d, $J = 8.3$ Hz, 2H), 7.62–7.59 (m, 2H), 7.55–7.51 (m, 1H), 7.24 (t, $J = 9.0$ Hz, 1H), 4.83 (s, 1H); ^{13}C NMR (150 MHz, DMSO-d_6) δ 163.1 (d, $J_{CF} = 243.6$ Hz), 159.3, 153.2, 149.6, 141.6 (d, $J_{CF} = 7.8$ Hz), 141.3, 136.2, 131.5 (d, $J_{CF} = 8.4$ Hz), 129.0, 126.7, 123.5, 115.5 (d, $J_{CF} = 20.7$ Hz), 114.2 (d, $J_{CF} = 22.3$ Hz), 96.6; HRMS-ESI(−) m/z calcd for $C_{16}H_{11}FN_2O_3S$ [M − H]$^-$ 329.0402, found 329.0398.

4.1.32. 6-((4'-chloro-[1,1'-biphenyl]-4-yl)thio)-3-hydroxypyrimidine-2,4(1H,3H)-dione (13g)

Yield 90%. White solid, m. p. > 250 °C; ^{1}H NMR (600 MHz, DMSO-d_6) δ 12.01 (s, 1H), 7.84 (d, $J = 8.1$ Hz, 2H), 7.77 (d, $J = 8.3$ Hz, 2H), 7.70 (d, $J = 8.1$ Hz, 2H), 7.55 (d, $J = 8.3$ Hz, 2H), 4.80 (s, 1H); ^{13}C NMR (150 MHz, DMSO-d_6) δ 159.3, 153.3, 149.6, 141.4, 137.9, 136.3, 133.7, 129.5, 129.2, 128.9, 126.3, 96.5; HRMS-ESI(−) m/z calcd for $C_{16}H_{11}ClN_2O_3S$ [M − H]$^-$ 345.0106, found 345.0108.

4.1.33. 3-Hydroxy-6-((4'-hydroxy-[1,1'-biphenyl]-4-yl)thio) pyrimidine-2,4(1H,3H)-dione (13h)

Yield 79%. White solid, m. p. 240–242 °C; ^{1}H NMR (600 MHz, DMSO-d_6) δ 11.95 (s, 1H), 10.34 (s, 1H), 9.68 (s, 1H), 7.74 (d, $J = 8.3$ Hz, 2H), 7.63 (d, $J = 8.3$ Hz, 2H), 7.57 (d, $J = 8.5$ Hz, 2H), 6.86 (d, $J = 8.6$ Hz, 2H), 4.74 (s, 1H); ^{13}C NMR (150 MHz, DMSO-d_6) δ 159.2, 158.3, 154.0, 149.5, 143.0, 136.4, 129.7, 128.6, 128.0, 124.2, 116.3, 96.0; HRMS-ESI(−) m/z calcd for $C_{16}H_{12}N_2O_4S$ [M − H]$^-$ 327.0445, found 327.0449.

4.1.34. 3-Hydroxy-6-((4'-methoxy-[1,1'-biphenyl]-4-yl)thio) pyrimidine-2,4(1H,3H)-dione (13i)

Yield 39%. White solid, m. p. 238–240 °C; ^{1}H NMR (600 MHz, CD$_3$OD) δ 7.66 (d, $J = 8.3$ Hz, 2H), 7.57 (d, $J = 8.3$ Hz, 2H), 7.53 (d, $J = 8.7$ Hz, 2H), 6.94 (d, $J = 8.7$ Hz, 2H), 4.89 (s, 1H), 3.75 (s, 3H); ^{13}C NMR (150 MHz, CD$_3$OD) δ 160.5, 160.1, 155.5, 149.6, 143.6, 135.9, 131.6, 127.92, 127.86, 123.8, 114.1, 95.4, 54.4; HRMS-ESI(−) m/z calcd for $C_{17}H_{14}N_2O_4S$ [M − H]$^-$ 341.0602, found 341.0598.

4.1.35. 3-Hydroxy-6-((3'-methoxy-[1,1'-biphenyl]-4-yl)thio) pyrimidine-2,4(1H,3H)-dione (13j)

Yield 57%. White solid, m. p. 225–227 °C; ^{1}H NMR (600 MHz, DMSO-d_6) δ 12.01 (s, 1H), 10.39 (s, 1H), 7.84 (d, $J = 8.1$ Hz, 2H), 7.69 (d, $J = 8.1$ Hz, 2H), 7.40 (t, $J = 7.9$ Hz, 1H), 7.29 (d, $J = 7.6$ Hz, 1H), 7.26 (s, 1H), 6.98 (d, $J = 8.2$ Hz, 1H), 4.78 (s, 1H), 3.82 (s, 3H); ^{13}C NMR (150 MHz, DMSO-d_6) δ 160.3, 159.3, 153.6, 149.6, 142.8, 140.6, 136.3, 130.6, 129.0, 125.9, 119.7, 114.5, 112.8, 96.3, 55.6; HRMS-ESI(−) m/z calcd for $C_{17}H_{14}N_2O_4S$ [M − H]$^-$ 341.0602, found 341.0596.

4.1.36. 6-((3',4'-dimethoxy-[1,1'-biphenyl]-4-yl)thio)-3-hydroxypyrimidine-2,4(1H,3H)-dione (13k)

Yield 59%. White solid, m. p. 185–187 °C; ^{1}H NMR (600 MHz, DMSO-d_6) δ 12.01 (s, 1H), 10.27 (s, 1H), 7.81 (d, $J = 7.9$ Hz, 2H), 7.65 (d, $J = 7.5$ Hz, 2H), 7.29 (s, 1H), 7.27 (d, $J = 8.9$ Hz, 1H), 7.05 (d, $J = 8.1$ Hz, 1H), 4.72 (s, 1H), 3.84 (s, 3H), 3.79 (s, 3H); ^{13}C NMR

(100 MHz, CD$_3$OD) δ 160.5, 155.5, 149.6, 149.5, 143.8, 135.9, 132.3, 128.2, 124.0, 119.6, 111.9, 110.6, 95.5, 55.2, 55.1; HRMS-ESI(−) *m/z* calcd for C$_{18}$H$_{16}$N$_2$O$_5$S [M − H]$^-$ 371.0707, found 371.0700.

4.1.37. 6-((3',5'-dimethoxy-[1,1'-biphenyl]-4-yl)thio)-3-hydroxypyrimidine-2,4(1H,3H)-dione (13l)

Yield 58%. White solid, m. p. 220−222 °C; ^{1}H NMR (600 MHz, CDCl$_3$) δ 7.65 (d, $J = 7.7$ Hz, 2H), 7.59 (d, $J = 7.3$ Hz, 2H), 6.70 (s, 2H), 6.52 (s, 1H), 5.46 (s, 1H), 3.86 (s, 6H); ^{13}C NMR (150 MHz, CDCl$_3$) δ 161.2, 158.6, 153.0, 151.5, 144.6, 141.4, 136.2, 129.3, 123.5, 105.5, 100.2, 96.0, 55.5; HRMS-ESI(−) *m/z* calcd for C$_{18}$H$_{16}$N$_2$O$_5$S [M − H]$^-$ 371.0707, found 371.0699.

4.1.38. 6-((4'-fluoro-3'-methyl-[1,1'-biphenyl]-4-yl)thio)-3-hydroxypyrimidine-2,4(1H,3H)-dione (13m)

Yield 70%. White solid, m. p. 186−188 °C; ^{1}H NMR (600 MHz, DMSO-d_6) δ 11.97 (s, 1H), 10.37 (s, 1H), 7.80 (d, $J = 8.2$ Hz, 2H), 7.69−7.67 (m, 3H), 7.60−7.57 (m, 1H), 7.24 (t, $J = 9.1$ Hz, 1H), 4.78 (s, 1H), 2.30 (s, 3H); ^{13}C NMR (150 MHz, DMSO-d_6) δ 161.4 (d, $J_{CF} = 244.8$ Hz), 159.2, 153.5, 149.5, 142.0, 136.3, 135.3, 130.8 (d, $J_{CF} = 5.3$ Hz), 128.8, 126.7 (d, $J_{CF} = 8.3$ Hz), 125.7, 125.4 (d, $J_{CF} = 17.5$ Hz), 116.0 (d, $J_{CF} = 22.4$ Hz), 96.3, 14.7; HRMS-ESI(−) *m/z* calcd for C$_{17}$H$_{13}$FN$_2$O$_3$S [M − H]$^-$ 343.0558, found 343.0563.

4.1.39. 6-((3'-fluoro-4'-methoxy-[1,1'-biphenyl]-4-yl)thio)-3-hydroxypyrimidine-2,4(1H,3H)-dione (13n)

Yield 61%. White solid, m. p. 205−207 °C; ^{1}H NMR (600 MHz, DMSO-d_6) δ 11.97 (s, 1H), 10.35 (s, 1H), 7.82 (d, $J = 8.3$ Hz, 2H), 7.67−7.65 (m, 3H), 7.56−7.55 (m, 1H), 7.28−7.25 (m, 1H), 4.78 (s, 1H), 3.88 (s, 3H); ^{13}C NMR (150 MHz, DMSO-d_6) δ 159.2, 153.6, 152.2 (d, $J_{CF} = 243.8$ Hz), 149.5, 147.8 (d, $J_{CF} = 10.7$ Hz), 141.3, 136.3, 131.9 (d, $J_{CF} = 6.5$ Hz), 128.5, 125.5, 123.6, 114.9, 114.7, 96.3, 56.6; HRMS-ESI(−) *m/z* calcd for C$_{17}$H$_{13}$FN$_2$O$_4$S [M − H]$^-$ 359.0507, found 359.0510.

4.1.40. 3-Hydroxy-6-((4'-(trifluoromethyl)-[1,1'-biphenyl]-3-yl)thio)pyrimidine-2,4(1H,3H)-dione (13o)

Yield 58%. White solid, m. p. 196−198 °C; ^{1}H NMR (600 MHz, DMSO-d_6) δ 11.97 (s, 1H), 10.36 (s, 1H), 8.00 (s, 1H), 7.96−7.93 (m, 3H), 7.83 (d, $J = 8.2$ Hz, 2H), 7.68−7.66 (m, 2H), 4.86 (s, 1H); ^{13}C NMR (150 MHz, DMSO-d_6) δ 159.3, 153.0, 149.6, 143.0, 140.9, 135.5, 134.0, 131.4, 129.8, 128.9 (q, $J_{CF} = 32.0$ Hz), 128.3, 128.2, 126.3 (q, $J_{CF} = 3.7$ Hz), 124.7 (q, $J_{CF} = 271.9$ Hz), 96.9; HRMS-ESI(−) *m/z* calcd for C$_{17}$H$_{11}$F$_3$N$_2$O$_3$S [M − H]$^-$ 379.0370, found 379.0363.

4.1.41. 3-Hydroxy-6-((3'-(trifluoromethyl)-[1,1'-biphenyl]-3-yl)thio)pyrimidine-2,4(1H,3H)-dione (13p)

Yield 72%. White solid, m. p. 195−197 °C; ^{1}H NMR (600 MHz, DMSO-d_6) δ 11.96 (s, 1H), 10.36 (s, 1H), 8.05−8.04 (m, 3H), 7.96 (d, $J = 7.7$ Hz, 1H), 7.76 (d, $J = 7.7$ Hz, 1H), 7.71 (t, $J = 7.7$ Hz, 1H), 7.67−7.64 (m, 2H), 4.84 (s, 1H); ^{13}C NMR (150 MHz, DMSO-d_6) δ 159.3, 153.2, 149.6, 140.9, 140.1, 135.3, 134.1, 131.5, 131.4, 130.6, 130.3 (q, $J_{CF} = 31.5$ Hz), 129.8, 128.1, 125.2 (q, $J_{CF} = 3.8$ Hz), 124.6 (q, $J_{CF} = 272.6$ Hz), 123.9 (q, $J_{CF} = 3.6$ Hz), 96.8; HRMS-ESI(−) *m/z* calcd for C$_{17}$H$_{11}$F$_3$N$_2$O$_3$S [M − H]$^-$ 379.0370, found 379.0370.

4.1.42. 6-((4'-fluoro-[1,1'-biphenyl]-3-yl)thio)-3-hydroxypyrimidine-2,4(1H,3H)-dione (13q)

Yield 80%. White solid, m. p. 168−170 °C; ^{1}H NMR (600 MHz, DMSO-d_6) δ 11.95 (s, 1H), 10.35 (s, 1H), 7.90 (s, 1H), 7.85 (d, $J = 6.9$ Hz, 1H), 7.78−7.76 (m, 2H), 7.63−7.60 (m, 2H), 7.32−7.29 (m, 2H), 4.83 (s, 1H); ^{13}C NMR (150 MHz, DMSO-d_6) δ 162.7 (d, $J_{CF} = 245.2$ Hz), 159.3, 153.3, 149.6, 141.5, 135.5 (d, $J_{CF} = 3.0$ Hz), 134.5, 133.6, 131.3, 129.5 (d, $J_{CF} = 8.2$ Hz), 129.4, 127.8, 116.3 (d, $J_{CF} = 21.4$ Hz), 96.7; HRMS-ESI(−) *m/z* calcd for C$_{16}$H$_{11}$FN$_2$O$_3$S [M − H]$^-$ 329.0402, found

329.0395.

4.1.43. 6-((3'-fluoro-[1,1'-biphenyl]-3-yl)thio)-3-hydroxypyrimidine-2,4(1H,3H)-dione (13r)

Yield 60%. White solid, m. p. 178−180 °C; ^{1}H NMR (600 MHz, DMSO-d_6) δ 11.95 (s, 1H), 10.37 (s, 1H), 7.97 (s, 1H), 7.92−7.90 (m, 1H), 7.64−7.57 (m, 4H), 7.53−7.50 (m, 1H), 7.23 (t, $J = 7.3$ Hz, 1H), 4.84 (s, 1H); ^{13}C NMR (150 MHz, DMSO-d_6) δ 163.1 (d, $J_{CF} = 243.6$ Hz), 159.3, 153.1, 149.6, 141.4 (d, $J_{CF} = 8.0$ Hz), 141.1, 135.1, 133.8, 131.5 (d, $J_{CF} = 8.4$ Hz), 131.3, 129.5, 128.0, 123.4, 115.3 (d, $J_{CF} = 21.1$ Hz), 114.2 (d, $J_{CF} = 22.4$ Hz), 96.8; HRMS-ESI(−) *m/z* calcd for C$_{16}$H$_{11}$FN$_2$O$_3$S [M − H]$^-$ 329.0402, found 329.0396.

4.1.44. 6-((4'-chloro-[1,1'-biphenyl]-3-yl)thio)-3-hydroxypyrimidine-2,4(1H,3H)-dione (13s)

Yield 82%. White solid, m. p. 190−192 °C; ^{1}H NMR (600 MHz, DMSO-d_6) δ 11.96 (s, 1H), 10.35 (s, 1H), 7.92 (s, 1H), 7.88−7.86 (m, 1H), 7.75 (d, $J = 8.5$ Hz, 2H), 7.63−7.62 (m, 2H), 7.53 (d, $J = 8.5$ Hz, 2H), 4.83 (s, 1H); ^{13}C NMR (150 MHz, DMSO-d_6) δ 159.3, 153.2, 149.6, 141.2, 137.8, 134.8, 133.6, 133.5, 131.3, 129.5, 129.4, 129.2, 128.0, 96.8; HRMS-ESI(−) *m/z* calcd for C$_{16}$H$_{11}$ClN$_2$O$_3$S [M − H]$^-$ 345.0106, found 345.0109.

4.1.45. 6-((3'-chloro-4'-fluoro-[1,1'-biphenyl]-3-yl)thio)-3-hydroxypyrimidine-2,4(1H,3H)-dione (13t)

Yield 70%. White solid, m. p. 185−187 °C; ^{1}H NMR (600 MHz, DMSO-d_6) δ 11.95 (s, 1H), 10.34 (s, 1H), 8.00−7.97 (m, 2H), 7.91−7.89 (m, 1H), 7.77−7.74 (m, 1H), 7.65−7.61 (m, 2H), 7.53−7.50 (m, 1H), 4.82 (s, 1H); ^{13}C NMR (150 MHz, DMSO-d_6) δ 159.3, 157.65 (d, $J_{CF} = 247.9$ Hz), 154.8, 149.6, 140.1, 136.8, 135.1, 133.8, 131.3, 129.52, 129.46, 128.1 (d, $J_{CF} = 7.4$ Hz), 120.7 (d, $J_{CF} = 17.8$ Hz), 117.9 (d, $J_{CF} = 21.2$ Hz), 96.7; HRMS-ESI(−) *m/z* calcd for C$_{16}$H$_{10}$ClFN$_2$O$_3$S [M − H]$^-$ 363.0012, found 363.0015.

4.1.46. 3-Hydroxy-6-((4'-(trifluoromethyl)-[1,1'-biphenyl]-2-yl)thio)pyrimidine-2,4(1H,3H)-dione (13u)

Yield 51%. White solid, m. p. 130−132 °C; ^{1}H NMR (600 MHz, DMSO-d_6) δ 11.77 (s, 1H), 10.30 (s, 1H), 7.79 (d, $J = 8.1$ Hz, 2H), 7.75 (d, $J = 7.8$ Hz, 1H), 7.68 (t, $J = 7.4$ Hz, 1H), 7.61−7.58 (m, 3H), 7.55 (d, $J = 7.5$ Hz, 1H), 4.67 (s, 1H); HRMS-ESI(−) *m/z* calcd for C$_{17}$H$_{11}$F$_3$N$_2$O$_3$S [M − H]$^-$ 379.0370, found 379.0370.

4.1.47. 6-((4'-fluoro-[1,1'-biphenyl]-2-yl)thio)-3-hydroxypyrimidine-2,4(1H,3H)-dione (13v)

Yield 55%. White solid, m. p. 135−137 °C; ^{1}H NMR (600 MHz, DMSO-d_6) δ 11.75 (s, 1H), 10.28 (s, 1H), 7.71 (d, $J = 7.8$ Hz, 1H), 7.64 (t, $J = 7.6$ Hz, 1H), 7.54 (t, $J = 7.6$ Hz, 1H), 7.50 (d, $J = 7.5$ Hz, 1H), 7.40−7.38 (m, 2H), 7.26−7.23 (m, 2H), 4.64 (s, 1H); HRMS-ESI(−) *m/z* calcd for C$_{16}$H$_{11}$FN$_2$O$_3$S [M − H]$^-$ 329.0402, found 329.0397.

5. Biology

5.1. Reagents

Biologicals. Recombinant HIV-1 reverse transcriptase (RT) was expressed and purified as previously described [30]. P4R5 HIV infection indicator cells were obtained from the NIH AIDS Reagent Program, Division of AIDS, NIAID, NIH (p4R5. MAGI from Dr. Nathaniel Landau). These cells express CD4, CXCR4 and CCR5 as well as a β-galactosidase reporter gene under the control of an HIV LTR promoter.

Chemicals. DNA and RNA oligonucleotides for the preparation of RNA/DNA duplexes for assay of RNase H activity were purchased from Trilink (San Diego, CA).

5.2. RNase H assay

RNase H activity was measured essentially as previously described [31]. RNA/DNA duplex substrate HTS-1 (RNA 5′-gaucu-gagccuggagcu -3′-fluorescein annealed to DNA 3′-CTA-GACTCGGACCCTCGA -5′-Dabcyl) is a high sensitivity duplex that assesses non-specific internal cleavage.

5.3. RT polymerase assay

RT pol assays [22,32–34] were carried out in 96-well plates by measuring the extension of an 18 nucleotide DNA primer (5′-GTCACTGTTCGAGCACCA-3′) annealed to a 100 nucleotide DNA template (5′-ATGTGTGTGCCCGTCTGTTGTGTGACTCTGGTAACTAGA-GATCCCTCAGACCCTTTTAGTCAGTGTGGAATATCTCA-TAGCTTGGTGCTCGAACAGTGAC-3′). Reactions containing 20 nM RT, 40 nM template/primer, and 10 μM deoxynucleotide triphosphates (dNTPs) in a buffer containing 50 mM Tris (pH 7.8) and 50 mM NaCl were initiated by the addition of 6 mM $MgCl_2$. Reactions contained 1% DMSO and increasing concentrations of compounds. DNA synthesis was carried out for 30 min at 37 °C, and reactions were arrested by the addition of 100 mM EDTA. The QuantiFluor dsDNA System (Promega) was used to quantify the amount of formed double-stranded DNA. Reactions were read at ex/em 504/531 nm in a PerkinElmer EnSpire Multilabel plate reader. Results were analyzed using Prism software (GraphPad Software, San Diego, CA) for nonlinear regression to fit dose-response data to logistic curve models.

5.4. HIV IN assay

HIV integrase was expressed and purified as previously reported [35]. Inhibition assays were performed using a modified protocol of our reported method [35]. Briefly, 2.1 μL of compound suspended in DMSO was placed in duplicate into a Black 96 well non-binding plate (corning 3991). Compounds were plated in duplicate to a final concentration of 0.13–100 μM. To each well of the plate 186.9 μL of reaction mixture without DNA substrate was added (10 mM HEPES pH 7.5, 10% glycerol w/v, 10 mM MnCl2, 1 mM DTT, 1 μM integrase). The enzyme was incubated with inhibitor for 10 min at 25 °C after which the reaction was initiated by the addition of 21 μL of 500 nM oligo (5′ biotin ATGTGGAAAATCTCTAGCA annealed with ACTGCTAGAGATTTTCCACAT 3′ Cy5). Reactions were incubated at 37 °C for 30 min and then quenched by the addition of 5.2 μL 500 mM EDTA. Each reaction was moved (200 μL) to a MultiScreen HTS PCR plate (Millipore MSSLBPC10) containing 20 μL streptavidin agarose beads (Life Technologies S951) and incubated with shaking for 30 min. A vacuum manifold was used to remove the reaction mixture and the beads were similarly washed 3 times with wash buffer (0.05% SDS, 1 mM EDTA in PBS). The plates were further washed 3 times with 200 μL 50 mM NaOH to denature DNA not covalently linked to the biotin modification. For each denaturation step the plate was incubated with shaking at 25 °C for 5 min and the NaOH was removed by centrifugation at 1000g for 1 min. The reaction products were eluted from the beads by the addition of 150 μL formamide. The plate was incubated at 25 °C for 10 min and read directly at 635/675 in a SpectraMax i3 plate reader (Molecular Devices).

5.5. Antiviral assays

MAGI assays were carried out using P4R5 indicator cells essentially as previously described [36]. P4R5 cells were cultured in 96-well microplates with 4×10^3 cells per well and maintained in DMEM/10% FBS supplemented with puromycin (1 μg/mL). Cells were incubated with either 1% DMSO or varying concentrations of the drugs for 24 h and then exposed to HIV-1 (MOI of 1.25) followed by an additional incubation period of 48 h. The extent of infection was assessed using a fluorescence-based β-galactosidase detection assay, as previously described with minor modifications [37]. After the 48 h incubation period, cells were lysed and 4-methylumbelliferylgalactoside (MUG) substrate was added. The β-galactosidase produced during infection acts on the MUG substrate and yields a fluorescent product, 4-methylumbelliferone (4-MU), that could be detected fluorimetrically with excitation wavelength 365 nm and emission wavelength 446 nm.

5.6. Parallel artificial membrane permeability assay (PAMPA)

The membrane permeability of selected compounds were evaluated using the Corning Gentest Pre-coated PAMPA Plate System (Cat. No. 353015). The pre-coated plate assembly, which was stored at −20 °C, was taken to thaw for 30 min at room temperature. The permeability assay was carried out in accordance with the manufacturer's protocol. In summary, the 96-well filter plate, pre-coated with lipids, was used as the permeation acceptor and a matching 96 well receiver plate was used as the permeation donor. Compound solutions were prepared by diluting 10 mM DMSO stock solutions in DPBS to a final concentration of 10 μM. The compound solutions were added to the wells (300 μL/well) of the receiver plate and DPBS was added to the wells (200 μL/well) of the pre-coated filter plate. The filter plate was then coupled with the receiver plate and the plate assembly was incubated at 25 °C without agitation for 5 h. At the end of the incubation, the plates were separated and the final concentrations of compounds in both donor wells and acceptor wells were analyzed using LC-MS/MS. Permeability of the compounds were calculated using the following formula:

$$P_e = \{-\ln [1-C_A(t)/C_{eq}]\}/[A \times (1/V_D+1/V_A) \times t]$$

where A = filter area (0.3 cm^2), V_D = donor well volume (0.3 mL), V_A = acceptor well volume (0.2 mL), t = incubation time (seconds), $C_A(t)$ = compound concentration in acceptor well at time t, $C_D(t)$ = compound concentration in donor well at time t, and $C_{eq} = [C_D(t) \times V_D + C_A(t) \times V_A]/(V_D + V_A)$.

5.7. Modeling and docking analysis

Molecular modeling was performed using the Schrödinger small molecule drug discovery suite 2014–3.

RNase H. The crystal structure of a hydroxypyridone carboxylic acid active-site RNase H inhibitor in complex with HIV Reverse Transcriptase was extracted from the Protein Data Bank (PDB code 5J1E [28]) as reported by Kankanala et al. [20]. The above structure was subjected to analysis and found that the native ligand, hydroxypyridone carboxylic acid was bound to the active site of RNase H. This model was subjected to Protein Preparation Wizard (Schrödinger Inc.) [38,39] in which missing hydrogens atoms were added, zero-order bonds to metals were created followed by the generation of metal binding states. The structure of protein was minimized using OPLS 2005 force field [40] to optimize hydrogen bonding network and converge heavy atoms to an rmsd of 0.3 Å. The processed model indicates that the interaction between the hydroxypyridone carboxylic acid and RNase H is mediated by two metal cations (Mg^{2+}) coordinated by the active site residues D443, E478, D498, and D549. The receptor grid generation tool in Maestro (Schrödinger Inc.) was used to define an active site around the native ligand to cover all the residues within 14 Å from it with both the metal cofactors (Mg^{2+}) as a constraint to identify the chelating

L. Wang et al. / European Journal of Medicinal Chemistry 156 (2018) 652–665

triad during docking.

Compound **13q** was drawn using Maestro and subjected to Lig Prep [41] to generate conformers, possible protonation at pH of 7 ± 3, and metal binding states that serve as an input for docking process. All the dockings were performed using Glide XP (Glide, version 6.4) [26,27] mode with both the Mg^{2+} metal cofactors as a constraint. The van der Waals radii of nonpolar atoms for each of the ligands were scaled by a factor of 0.8. The predicted binding mode of compounds **13q** features the critical interaction between the chelating triad and to the divalent metal cofactors. The ligand within the active site of RNase H was further refined post docking by minimizing under implicit solvent to account for the local protein flexibility.

PFV integrase. Compound **13q** was docked into the active site of the retroviral PFV integrase. The crystal structure of PFV intasome in complex with magnesium and Dolutegravir was used as a starting point (PDB code: 3S3M [29]) for both the protein preparation and the receptor grid generation. The protocol is followed in an identical manner as reported above for RNase H. Compound **13q** was prepared using Lig Prep and docked into the active site of PFV intasome crystal structure.

PDB ID

The atomic coordinates and structure factors have been deposited in the RCSB Protein Data Bank (PDB ID: 5J1E, 3S3M). Authors will release the atomic coordinates and experimental data upon article publication.

Acknowledgements

Abbreviations

HIV	human immunodeficiency virus
RT	reverse transcriptase
RNase H	ribonuclease H
HPD	3-hydroxypyrimidine-2,4-dione
Pol	polymerase
INST	integrase strand transfer
IN	integrase
PR	protease
HAART	highly active antiretroviral therapy
NRTIs	nucleoside RT inhibitors
NNRTIs	nonnucleoside RT inhibitors
HID	2-hydroxyisoquinolinedione
DKA	diketoacid
HPCA	hydroxypyridonecarboxylic acid
SAR	structure-activity-relationship

Appendix A. Supplementary data

Supplementary data related to this article can be found at https://doi.org/10.1016/j.ejmech.2018.07.039.

References

[1] T. Cihlar, M. Fordyce, Current status and prospects of HIV treatment, Curr. Opin. Virol. 18 (2016) 50–56.
[2] C. Stephan, A. Hill, W. Sawyer, Y. van Delft, C. Moecklinghoff, Impact of baseline HIV-1 RNA levels on initial highly active antiretroviral therapy outcome: a meta-analysis of 12,370 patients in 21 clinical trials*, HIV Med. 14 (2013) 284–292.
[3] S.G. Sarafianos, B. Marchand, K. Das, D.M. Himmel, M.A. Parniak, S.H. Hughes, E. Arnold, Structure and function of HIV-1 reverse transcriptase: molecular mechanisms of polymerization and inhibition, J. Mol. Biol. 385 (2009) 693–713.
[4] T. Cihlar, A.S. Ray, Nucleoside and nucleotide HIV reverse transcriptase inhibitors: 25 years after zidovudine, Antivir. Res. 85 (2010) 39–58.
[5] M.P. de Bethune, Non-nucleoside reverse transcriptase inhibitors (NNRTIs), their discovery, development, and use in the treatment of HIV-1 infection: a review of the last 20 years (1989-2009), Antivir. Res. 85 (2010) 75–90.
[6] G.L. Beilhartz, M. Gotte, HIV-1 ribonuclease H: structure, catalytic mechanism and inhibitors, Viruses 2 (2010) 900–926.
[7] M. Tisdale, T. Schulze, B.A. Larder, K. Moelling, Mutations within the RNase H domain of human immunodeficiency virus type 1 reverse transcriptase abolish virus infectivity, J. Gen. Virol. 72 (1991) 59–66.
[8] L. Cao, W. Song, E. De Clercq, P. Zhan, X. Liu, Recent progress in the research of small molecule HIV-1 RNase H inhibitors, Curr. Med. Chem. 21 (2014) 1956–1967.
[9] K. Klumpp, J.Q. Hang, S. Rajendran, Y.L. Yang, A. Derosier, P.W.K. In, H. Overton, K.E.B. Parkes, N. Cammack, J.A. Martin, Two-metal ion mechanism of RNA cleavage by HIV RNase H and mechanism-based design of selective HIV RNase H inhibitors, Nucleic Acids Res. 31 (2003) 6852–6859.
[10] D.M. Himmel, K.A. Maegley, T.A. Pauly, J.D. Bauman, K. Das, C. Dharia, A.D. Clark Jr., K. Ryan, M.J. Hickey, R.A. Love, S.H. Hughes, S. Bergqvist, E. Arnold, Structure of HIV-1 reverse transcriptase with the inhibitor beta-Thujaplicinol bound at the RNase H active site, Structure 17 (2009) 1625–1635.
[11] D.M. Himmel, N.S. Myshakina, T. Ilina, A. Van Ry, W.C. Ho, M.A. Parniak, E. Arnold, Structure of a dihydroxycoumarin active-site inhibitor in complex with the RNase H domain of HIV-1 reverse transcriptase and structure-activity analysis of inhibitor analogs, J. Mol. Biol. 426 (2014) 2617–2631.
[12] C.A. Shaw-Reid, V. Munshi, P. Graham, A. Wolfe, M. Witmer, R. Danzeisen, D.B. Olsen, S.S. Carroll, M. Embrey, J.S. Wai, M.D. Miller, J.L. Cole, D.J. Hazuda, Inhibition of HIV-1 ribonuclease H by a novel diketo acid, 4-[5-(benzoylamino)thien-2-yl]-2,4-dioxobutanoic acid, J. Biol. Chem. 278 (2003) 2777–2780.
[13] T.A. Kirschberg, M. Balakrishnan, N.H. Squires, T. Barnes, K.M. Brendza, X. Chen, E.J. Eisenberg, W. Jin, N. Kutty, S. Leavitt, A. Liclican, Q. Liu, X. Liu, J. Mak, J.K. Perry, M. Wang, W.J. Watkins, E.B. Lansdon, RNase H active site inhibitors of human immunodeficiency virus type 1 reverse transcriptase: design, biochemical activity, and structural information, J. Med. Chem. 52 (2009) 5781–5784.
[14] P.D. Williams, D.D. Staas, S. Venkatraman, H.M. Loughran, R.D. Ruzek, T.M. Booth, T.A. Lyle, J.S. Wai, J.P. Vacca, B.P. Feuston, L.T. Ecto, J.A. Flynn, D.J. DiStefano, D.J. Hazuda, C.M. Bahnck, A.L. Himmelberger, G. Dornadula, R.C. Hrin, K.A. Stillmock, M.V. Witmer, M.D. Miller, J.A. Grobler, Potent and selective HIV-1 ribonuclease H inhibitors based on a 1-hydroxy-1,8-naphthyridin-2(1H)-one scaffold, Bioorg. Med. Chem. Lett 20 (2010) 6754–6757.
[15] G.L. Beilhartz, M. Ngure, B.A. Johns, F. Deanda, P. Gerondelis, M. Gotte, Inhibition of the ribonuclease H activity of HIV-1 reverse transcriptase by GSK5750 correlates with slow enzyme-inhibitor dissociation, J. Biol. Chem. 289 (2014) 16270–16277.
[16] M. Nowotny, Retroviral integrase superfamily: the structural perspective, EMBO Rep. 10 (2009) 144–151.
[17] Y. Li, S. Xuan, Y. Feng, A. Yan, Targeting HIV-1 integrase with strand transfer inhibitors, Drug Discov. Today 20 (2015) 435–449.
[18] D.J. McColl, X. Chen, Strand transfer inhibitors of HIV-1 integrase: bringing IN a new era of antiretroviral therapy, Antivir. Res. 85 (2010) 101–118.
[19] S.K. Vernekar, Z. Liu, E. Nagy, L. Miller, K.A. Kirby, D.J. Wilson, J. Kankanala, S.G. Sarafianos, M.A. Parniak, Z. Wang, Design, synthesis, biochemical, and antiviral evaluations of C6 benzyl and C6 biarylmethyl substituted 2-hydroxylisoquinoline-1,3-diones: dual inhibition against HIV reverse transcriptase-associated RNase H and polymerase with antiviral activities, J. Med. Chem. 58 (2015) 651–664.
[20] J. Kankanala, K.A. Kirby, F. Liu, L. Miller, E. Nagy, D.J. Wilson, M.A. Parniak, S.G. Sarafianos, Z.Q. Wang, Design, synthesis, and biological evaluations of hydroxypyridonecarboxylic acids as inhibitors of HIV reverse transcriptase associated RNase H, J. Med. Chem. 59 (2016) 5051–5062.
[21] J. Tang, F. Liu, E. Nagy, L. Miller, K.A. Kirby, D.J. Wilson, B.L. Wu, S.G. Sarafianos, M.A. Parniak, Z. Wang, 3-Hydroxypyrimidine-2,4-diones as selective active site inhibitors of HIV reverse transcriptase-associated RNase H: design, synthesis, and biochemical evaluations, J. Med. Chem. 59 (2016) 2648–2659.
[22] J. Kankanala, K.A. Kirby, A.D. Huber, M.C. Casey, D.J. Wilson, S.G. Sarafianos, Z.Q. Wang, Design, synthesis and biological evaluations of N-Hydroxy thienopyrimidine-2,4-diones as inhibitors of HIV reverse transcriptase-associated RNase H, Eur. J. Med. Chem. 141 (2017) 149–161.
[23] F. Yoneda, K. Tsukuda, M. Kawazoe, A. Sone, Synthesis and properties of 1-benzothiopyrano[2,3-d]-pyrimidine-2,4-(3h)diones (10-thia-5-deazaflavins), J. Heterocycl. Chem. 18 (1981) 1329–1334.
[24] N. Miyaura, A. Suzuki, Palladium-catalyzed cross-coupling reactions of organoboron compounds, Chem. Rev. 95 (1995) 2457–2483.
[25] A.L. Hopkins, J.S. Ren, J. Tanaka, M. Baba, M. Okamato, D.I. Stuart, D.K. Stammers, Design of MKC-442 (emivirine) analogues with improved activity against drug-resistant HIV mutants, J. Med. Chem. 42 (1999) 4500–4505.

[26] Small-Molecule Drug Discovery Suite 2014-3: Glide, Version 6.4, Schrödinger, LLC, New York, 2014.

[27] R.A. Friesner, R.B. Murphy, M.P. Repasky, L.L. Frye, J.R. Greenwood, T.A. Halgren, P.C. Sanschagrin, D.T. Mainz, Extra precision glide: docking and scoring incorporating a model of hydrophobic enclosure for protein-ligand complexes, J. Med. Chem. 49 (2006) 6177–6196.

[28] http://www.rcsb.org/pdb/explore/explore.do?structureId=5J1E.

[29] S. Hare, S.J. Smith, M. Metifiot, A. Jaxa-Chamiec, Y. Pommier, S.H. Hughes, P. Cherepanov, Structural and functional analyses of the second-generation integrase strand transfer inhibitor dolutegravir (S/GSK1349572), Mol. Pharmacol. 80 (2011) 565–572.

[30] R.S. Fletcher, G. Holleschak, E. Nagy, D. Arion, G. Borkow, Z. Gu, M.A. Wainberg, M.A. Parniak, Single-step purification of recombinant wild-type and mutant HIV-1 reverse transcriptase, Protein Expres. Purif. 7 (1996) 27–32.

[31] M.A. Parniak, K.L. Min, S.R. Budihas, S.F. Le Grice, J.A. Beutler, A fluorescence-based high-throughput screening assay for inhibitors of human immunodeficiency virus-1 reverse transcriptase-associated ribonuclease H activity, Anal. Biochem. 322 (2003) 33–39.

[32] J. Tang, K.A. Kirby, A.D. Huber, M.C. Casey, J. Ji, D.J. Wilson, S.G. Sarafianos, Z.Q. Wang, 6-Cyclohexylmethyl-3-hydroxypyrimidine-2,4-dione as an inhibitor scaffold of HIV reverase transcriptase: impacts of the 3-OH on inhibiting RNase H and polymerase, Eur. J. Med. Chem. 128 (2017) 168–179.

[33] S.K.V. Vernekar, J. Tang, B. Wu, A.D. Huber, M.C. Casey, N. Myshakina, D.J. Wilson, J. Kankanala, K.A. Kirby, M.A. Parniak, S.G. Sarafianos, Z. Wang, Double-winged 3-hydroxypyrimidine-2,4-diones: potent and selective inhibition against HIV-1 RNase H with significant antiviral activity, J. Med. Chem.

[34] 60 (2017) 5045–5056.

K. Singh, B. Marchand, D.K. Rai, B. Sharma, E. Michailidis, E.M. Ryan, K.B. Matzek, M.D. Leslie, A.N. Hagedorn, Z. Li, P.R. Norden, A. Hachiya, M.A. Parniak, H.T. Xu, M.A. Wainberg, S.G. Sarafianos, Biochemical mechanism of HIV-1 resistance to rilpivirine, J. Biol. Chem. 287 (2012) 38110–38123.

[35] Z. Wang, E.M. Bennett, D.J. Wilson, C. Salomon, R. Vince, Rationally designed dual inhibitors of HIV reverse transcriptase and integrase, J. Med. Chem. 50 (2007) 3416–3419.

[36] V.R. Sirivolu, S.K.V. Vernekar, T. Ilina, N.S. Myshakina, M.A. Parniak, Z.Q. Wang, Clicking 3'-azidothymidine into novel potent inhibitors of human immunodeficiency virus, J. Med. Chem. 56 (2013) 8765–8780.

[37] M.E. Abram, M.A. Parniak, Virion instability of human immunodeficiency virus type 1 reverse transcriptase (RT) mutated in the protease cleavage site between RT p51 and the RT RNase H domain, J. Virol. 79 (2005) 11952–11961.

[38] G.M. Sastry, M. Adzhigirey, T. Day, R. Annabhimoju, W. Sherman, Protein and ligand preparation: parameters, protocols, and influence on virtual screening enrichments, J. Comput. Aided Mol. Des. 27 (2013) 221–234.

[39] Schrödinger Release 2014-3: Schrödinger Suite 2014-3 Protein Preparation Wizard; Epik Version 2.9, Schrödinger, LLC, New York, NY, 2014; Impact Version 6.4, Schrödinger, LLC, New York, NY, 2014; Prime Version 3.7, Schrödinger, LLC, New York, NY, 2014.

[40] W.L. Jorgensen, D.S. Maxwell, J. TiradoRives, Development and testing of the OPLS all-atom force field on conformational energetics and properties of organic liquids, J. Am. Chem. Soc. 118 (1996) 11225–11236.

[41] Schrödinger Release 2014-3, LigPrep, Version 3.1, Schrödinger, LLC, New York, NY, 2014.